UNIVERSIDAD DE CASTILLA - LA MANCHA

ESCUELA DE INGENIERÍA INDUSTRIAL DE TOLEDO

DEPARTAMENTO DE INGENIERÍA ELÉCTRICA,
ELECTRÓNICA, AUTOMÁTICA Y COMUNICACIONES

CARACTERIZACIÓN DEL COMPORTAMIENTO ELÉCTRICO PASIVO DE TEJIDOS EXCITABLES Y NO EXCITABLES DE ROEDOR UTILIZANDO LA TÉCNICA DE INTERRUPCIÓN DE CORRIENTE Y MEDIDAS DE IMPEDANCIA

TESIS DOCTORAL

AUTOR: ENRIQUE HERNÁNDEZ BALAGUERA

DIRECTORES: JOSÉ LUIS POLO SANZ
ELISA LÓPEZ DOLADO

Toledo, abril de 2019

Índice

1 Resumen y organización de la memoria **1**

2 Introducción **5**
2.1 Aspectos específicos sobre teoría de circuitos y bioimpedancia 7
2.1.1 Elemento de fase constante (CPE) 8
2.1.2 Respuesta natural de circuitos R-CPE ($0<\alpha<1$) 9
2.2 Bibliografía 10

3 Objetivos **13**

4 Discusión conjunta y artículos publicados **17**
4.1 Discusión conjunta 19
4.2 Artículos publicados 20
4.2.1 Artículo nº 1 21
4.2.2 Artículo nº 2 35
4.2.3 Artículo nº 3 45

5 Conclusiones y futuros desarrollos **57**
5.1 Conclusiones 59
5.2 Sugerencias sobre futuros desarrollos 60

Capítulo 1

Resumen y organización de la memoria

1 Resumen y organización de la memoria

El interés biológico en el conocimiento del comportamiento eléctrico pasivo de los tejidos reside en la determinación de su estado fisiológico. Una forma de caracterizar dicho comportamiento eléctrico consiste en la obtención secuencial de medidas de impedancia eléctrica: la impedancia se mide a una frecuencia determinada hasta cubrir un rango de frecuencias de interés (espectroscopía de impedancia eléctrica). En este caso, la obtención del espectro de impedancia consume un tiempo que puede ser crítico cuando se analizan estados tisulares que cambian muy rápidamente y que, por tanto, no pueden considerarse invariantes en el tiempo durante el período de adquisición de la medida. Por tanto, la obtención rápida de medidas eléctricas supone una estrategia para la monitorización en tiempo real del estado fisiológico de los tejidos y detección de cambios rápidos, y además el medio biológico se encuentra menos tiempo perturbado.

En la actualidad, las ideas o técnicas de la teoría de circuitos han trascendido a otras ramas de la ciencia como, por ejemplo, su aplicación en biofísica y bioelectricidad, resultando cruciales en la explicación y resolución de sus propios problemas. Además, la introducción de herramientas matemáticas avanzadas, como el cálculo diferencial e integral de orden no entero, permiten describir matemáticamente el comportamiento de componentes y circuitos eléctricos complejos.

En el presente trabajo de investigación, se han obtenido circuitos eléctricos equivalentes (EECs) de tejidos biológicos de roedor, tanto *ex vivo* (tejidos extraídos del animal después de la perfusión y el sacrificio) como *in vivo* (con el animal anestesiado), mediante la técnica de interrupción de corriente. Las propiedades capacitivas del tejido se modelan utilizando el elemento eléctrico distribuido denominado "elemento de fase constante" (CPE), por lo que se hace necesaria la introducción del cálculo fraccionario para la estimación de los parámetros eléctricos. Específicamente, se ha analizado la potencialidad de la técnica de interrupción de corriente en la monitorización *in vivo* y detección de diferencias en los parámetros eléctricos de tejidos excitables responsables de la función motriz -médula espinal y músculos estriados-. Dicho estudio supone un paso previo a analizar sus usos potenciales en las lesiones de la médula espinal, tanto en lo referente a la recuperación funcional como en lo que atañe a la mejora técnica en el diagnóstico clínico del déficit sensitivo y motor en sí. Los resultados obtenidos suponen un avance en el conocimiento de las propiedades eléctricas específicas y diferenciales del tejido neural, ya que permitirían optimizar el diseño de las neuroprótesis implantables crónicamente y mejorar la bioseguridad y eficacia de los protocolos de estimulación eléctrica. Finalmente, con vistas a su aplicación en la caracterización del comportamiento eléctrico pasivo de tejidos biológicos, se propone una generalización del método de inyección súbita de carga (método "culostático") utilizando un CPE.

El Capítulo 2 presenta algunos aspectos específicos sobre teoría de circuitos y bioimpedancia que son de interés en el presente trabajo de investigación. Se analiza el CPE, su tratamiento matemático en el dominio del tiempo y la respuesta natural de circuitos resistivos que contienen un CPE actuando como condensador fraccionario.

El Capítulo 3 establece los objetivos que se persiguen en la presente investigación.

En el Capítulo 4 se incluyen los artículos en revistas indexadas (JCR) a los que ha dado lugar el presente trabajo de investigación, así como una discusión conjunta.

El Capítulo 5 presenta las conclusiones alcanzadas y futuras líneas de trabajo.

Capítulo 2

Introducción

2 Introducción

Este Capítulo presenta algunos aspectos específicos sobre teoría de circuitos y bioimpedancia que son de interés en el presente trabajo de investigación. Se analiza el elemento de fase constante (CPE), su tratamiento matemático en el dominio del tiempo y la respuesta natural de circuitos resistivos que contienen un CPE actuando como condensador fraccionario. Remítase también el lector a las introducciones de cada uno de los tres artículos que se anexan en el Capítulo 4.

2.1 Aspectos específicos sobre teoría de circuitos y bioimpedancia

El conocimiento de las propiedades eléctricas de los tejidos es de gran interés en un amplio abanico de aplicaciones biomédicas [1-3]. Específicamente, dichas propiedades eléctricas determinan el tipo de tejido [4-6], su estado fisiológico [7-9] o, en la práctica clínica, permiten evaluar el posible efecto terapéutico de tratamientos [10] tales como la estimulación eléctrica funcional. La reconstrucción de imágenes médicas basadas en las propiedades eléctricas de los tejidos, tomografía de impedancia eléctrica (EIT) [2,11,12], resulta de utilidad en la visualización anatómica, actividad fisiológica y diagnóstico [13].

La caracterización del comportamiento eléctrico pasivo de un tejido puede realizarse midiendo su impedancia (bioimpedancia), es decir, la oposición que presenta al paso de la corriente eléctrica alterna en un rango de frecuencias de interés [1,14-16]. Específicamente, dentro de la dispersión frecuencial β (kilohercios a megahercios) se puede observar el mecanismo de carga/descarga de las membranas celulares (que poseen comportamiento capacitivo), a través de los medios intra- y extracelular (con comportamiento resistivo -son soluciones electrolíticas-), para los diversos tipos de tejidos [1,17]. Este mecanismo de carga/descarga refleja cambios estructurales en las membranas, lo que puede resultar de relevancia clínica.

En general, un circuito eléctrico equivalente (EEC) que describe datos experimentales de bioimpedancia requiere la utilización de elementos eléctricos distribuidos [18,19]. En efecto, los elementos básicos (tales como resistencias, condensadores o bobinas) que se utilizan en teoría de circuitos poseen una localización puntual y se comportan de manera ideal en todo el espectro de frecuencias. Sin embargo, un tejido o una interfase electrodo/tejido ocupan una región en el espacio y sus propiedades eléctricas se encuentran "repartidas" (distribuidas) en dicha región [18].

Cole proporcionó una fórmula empírica que permite modelar las medidas de impedancia obtenidas en tejidos biológicos [20]. Dicha expresión se corresponde con un EEC formado por dos resistencias y un CPE, que es un elemento eléctrico distribuido capaz de modelar las propiedades capacitivas del tejido [21]. A continuación se analiza dicho elemento y la respuesta natural de un circuito constituido por resistencias y un CPE (circuitos R-CPE).

2.1.1 Elemento de fase constante (CPE)

La impedancia Z(s) del elemento de fase constante (CPE) se expresa como [22]:

$$Z_Q(s)=\frac{1}{Qs^{\alpha}} \tag{1}$$

donde Q y α son la magnitud y el exponente del CPE, respectivamente; s es la variable de Laplace. Para los valores -1, 0 y 1 del parámetro α, la ecuación del CPE se reduce a una bobina (L=1/Q), una resistencia (R=1/Q) y un condensador (C=Q), ideales, respectivamente. Para frecuencias físicas s=jω (ω es la pulsación con ω=2πf, donde f es la frecuencia; j es la unidad imaginaria), la impedancia de la Ecuación (1), presenta un ángulo de valor $-\alpha\pi/2$ que es constante con la frecuencia (de ahí el nombre de "elemento de fase constante") [18].

El interés del CPE en el presente trabajo de investigación es cuando actúa como condensador fraccionario y por ello se considera el rango $0<\alpha<1$. La Ecuación (1) puede escribirse como $I_Q(s)=Qs^{\alpha}V_Q(s)$ donde $V_Q(s)$ e $I_Q(s)$ son las transformadas de Laplace de la tensión y corriente del CPE, respectivamente. En el dominio del tiempo se tiene:

$$i_Q(t)=Q\frac{d^{\alpha}v_Q(t)}{dt^{\alpha}};\quad 0<\alpha<1 \tag{2}$$

donde las unidades de Q son faradios×(segundos)$^{\alpha-1}$ en el Sistema Internacional de Unidades [23]. La Ecuación (2) muestra una generalización de la ecuación característica del condensador en la que la relación entre la tensión $v_Q(t)$ y la corriente $i_Q(t)$ puede expresarse utilizando una derivada de orden α no entero ($0<\alpha<1$) [23].

Análogamente, la Ecuación (1) puede también escribirse como $V_Q(s)=(1/(Qs^{\alpha}))I_Q(s)$. Utilizando la operación de convolución (*) es posible escribir en el dominio del tiempo [24,25]:

$$v_Q(t)=\frac{1}{Q}L^{-1}\left[\frac{1}{s^{\alpha}}\right]*i_Q(t)=\frac{1}{Q}\frac{t^{\alpha-1}}{\Gamma(\alpha)}*i_Q(t)=\frac{1}{Q}\frac{1}{\Gamma(\alpha)}\int_0^t(t-\tau)^{\alpha-1}i_Q(\tau)d\tau \tag{3}$$

donde Γ es la función gamma y L^{-1} representa la transformada inversa de Laplace. La integral de convolución de la Ecuación (3) es, en realidad, la integral fraccionaria de Riemann-Liouville [25] y permite expresar, en el dominio el tiempo, la tensión del CPE como la integral fraccionaria de su corriente. Si $\alpha\rightarrow1$, la función de peso en la integral de convolución $(t-\tau)^{\alpha-1}/\Gamma(\alpha)\rightarrow u(t-\tau)$ -u(t) es la función escalón unitario- y la Ecuación (3) describe el comportamiento de un condensador ideal.

A partir de la Ecuación (2) o la Ecuación (3) es posible demostrar que, bajo la aplicación de un escalón de tensión, la carga (integral de la corriente $i_Q(t)$) en un condensador fraccionario, crece indefinidamente con el tiempo según una ley potencial [23]. Sin embargo, en el condensador ideal, la aplicación de un escalón de tensión proporciona una corriente impul-

siva y, por tanto, una carga instantánea del condensador al producto de su capacidad y tensión aplicada.

2.1.2 Respuesta natural de circuitos R-CPE (0<α<1)

La Ecuación (4) presenta una ecuación diferencial lineal, homogénea, de coeficientes constantes y fraccionaria con 0<α<1; x(t) es la variable de interés o salida.

$$\frac{d^{\alpha}x(t)}{dt^{\alpha}}+\frac{x(t)}{\tau^{\alpha}}=0\ ;\quad 0<\alpha<1 \tag{4}$$

En el Sistema Internacional de Unidades, la constante de tiempo τ se expresa en segundos y se encuentra elevada al exponente α para mantener la consistencia de unidades en la Ecuación (4). En teoría de circuitos, la Ecuación (4) modela un circuito resistivo que incluye un CPE actuando como condensador fraccionario. En este caso, la constante de tiempo τ puede obtenerse por inspección desde el circuito R-CPE (0<α<1) como:

$$\tau=(R_{Th}Q)^{1/\alpha} \tag{5}$$

donde R_{Th}, es la resistencia de Thévenin que "ve" el CPE entre sus bornes.

La Ecuación (4) puede ser resuelta, por ejemplo, tomando la derivada en el sentido de Caputo y aplicando la transformada de Laplace [23,25]. La función de Mittag-Leffler $E_{\alpha}[-(t/\tau)^{\alpha}]$, definida por la serie convergente de la Ecuación (6), constituye la base de soluciones de dicha Ecuación (4).

$$E_{\alpha}[-(t/\tau)^{\alpha}]=\sum_{k=0}^{\infty}\frac{[-(t/\tau)^{\alpha}]^{k}}{\Gamma(\alpha k+1)} \tag{6}$$

En el caso de α=1, la Ecuación (6) proporciona el desarrollo de MacLaurin de la función exponencial (base de soluciones de la Ecuación (4) para α=1): $E_1[-(t/\tau)]=\exp[-(t/\tau)]$.

La Ecuación (6) indica que el comportamiento del circuito R-CPE (0<α<1) depende de la escala de tiempos considerada. Específicamente, la Ecuación (7) muestra dos escalas de tiempo bien diferenciadas [26]: (i) un régimen de tiempos cortos que se aproxima al comportamiento de una función exponencial de argumento proporcional a t^{α} ("stretched exponential") y (ii) un régimen de tiempos largos, aproximado por una función potencial inversa de exponente α.

$$E_{\alpha}[-(t/\tau)^{\alpha}]\sim\begin{cases}1-\dfrac{(t/\tau)^{\alpha}}{\Gamma(\alpha+1)}+\ldots\sim\exp\left[-\dfrac{(t/\tau)^{\alpha}}{\Gamma(\alpha+1)}\right], & (t/\tau)\to 0^{+}\\ \dfrac{(t/\tau)^{-\alpha}}{\Gamma(1-\alpha)}\sim\dfrac{\operatorname{sen}(\alpha\pi)}{\pi}\left(\dfrac{\tau}{t}\right)^{\alpha}\Gamma(\alpha), & (t/\tau)\to\infty\end{cases} \tag{7}$$

La Figura 1 dibuja la función de Mittag-Leffler en comparación con la función exponencial. La función de Mittag-Leffler interpola entre los dos regímenes de tiempo anteriormente indicados, presentando una caída brusca para tiempos cortos (más rápida que la corres-

pondiente a la función exponencial), y una cola larga con un decrecimiento mucho más lento que la exponencial, para tiempos largos.

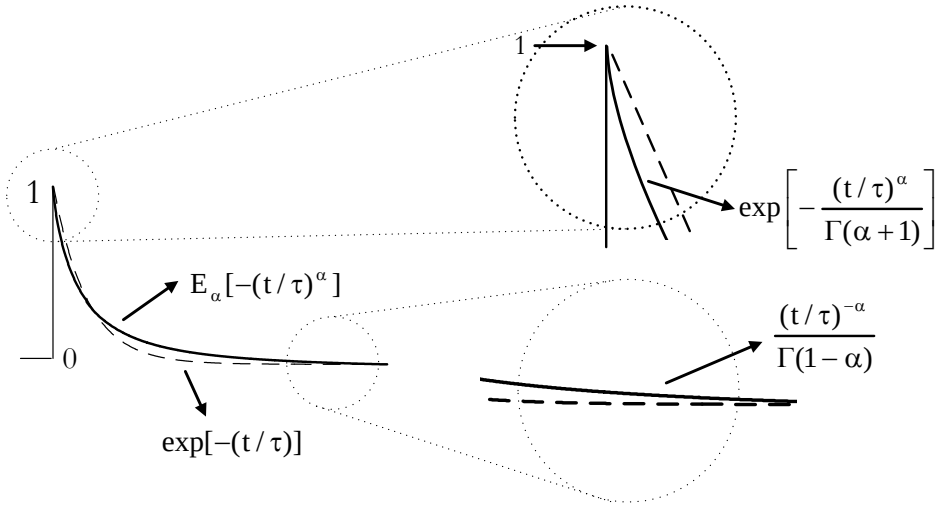

Figura 1. Representación de la función de Mittag-Leffler (línea continua) frente a la función exponencial (línea discontinua). Las magnificaciones de la curva muestran los dos regímenes de tiempo indicados en el texto.

2.2 Bibliografía

[1] S. Grimnes, O. G. Martinsen. "Bioimpedance and bioelectricity basics" *Academic Press*, 2015.

[2] F. Simini, P. Bertemes-Filho. "Bioimpedance in biomedical applications and research" *Springer*, 2018.

[3] T. K. Bera. "Bioelectrical impedance methods for noninvasive health monitoring: A review" *Journal of Medical Engineering* 2014 (2014) 381251.

[4] C. Gabriel, S. Gabriel, E. Corthout. "The dielectric properties of biological tissues: I. Literature survey" *Physics in Medicine and Biology* 41(11) (1996) 2231-2249.

[5] S. Gabriel, R. W. Lau, C. Gabriel. "The dielectric properties of biological tissues: II. Measurements in the frequency range 10 Hz to 20 GHz" *Physics in Medicine and Biology* 41(11) (1996) 2251-2269.

[6] S. Gabriel, R. W. Lau, C. Gabriel. "The dielectric properties of biological tissues: III. Parametric models for the dielectric spectrum of tissues" *Physics in Medicine and Biology* 41(11) (1996) 2271-2293.

[7] O. Casas, R. Bragós, P. J. Riu, J. Rosell, M. Tresànchez, M. Warren, A. Rodríguez-Sinovas, A. Carreño, J. Cinca. "*In vivo* and *in situ* ischemic tissue characterization using electrical impedance spectroscopy" *Annals of the New York Academy of Sciences* 873 (1999) 51-58.

[8] S. Laufer, A. Ivorra, V. E. Reuter, B. Rubinsky, S. B. Solomon. "Electrical impedance characterization of normal and cancerous human hepatic tissue" *Physiological Measurements* 31(7) (2010) 995-1009.

[9] E. Gersing. "Impedance spectroscopy on living tissue for determination of the state of organs" *Bioelectrochemistry and Bioenergetics* 45(2) (1998) 145-149.

[10] J. P. Reilly, H. Antoni, M. A. Chilbert, J. D. Sweeney. "Applied bioelectricity: From electrical stimulation to electropathology" *Springer*, 1998.

[11] R. H. Bayford. "Bioimpedance tomography (Electrical Impedance Tomography)" *Annual Review of Biomedical Engineering* 8 (2006) 63-91.

[12] D. S. Holder. "Electrical Impedance Tomography: Methods, history and applications" *Institute of Physics Publishing Ltd.*, 2005.

[13] T. K. Bera. "Applications of Electrical Impedance Tomography (EIT): A short review" *IOP Conference Series: Materials Science and Engineering* 331 (2018) 012004.

[14] E. T. McAdams, J Jossinet. "Tissue impedance: A historical overview" *Physiological Measurements* 16 (1995) A1-A13.

[15] B. Rigaud, J. P. Morucci, N. Chauveau. "Bioelectrical impedance techniques in medicine. Part I: Bioimpedance Measurement. Second section: Impedance spectrometry" *Critical Reviews in Biomedical Engineering* 24(4-6) (1996) 257-351.

[16] J. J. Ackmann, M. A. Seitz. "Methods of complex impedance measurements in biologic tissue" *Critical Reviews in Biomedical Engineering* 11(4) (1984) 281-311.

[17] H. P. Schwan. "Electrical properties of tissues and cell suspensions" *Advances in Biological and Medical Physics* 5 (1957) 147-209.

[18] E. Barsoukov, J. R. Macdonald. "Impedance Spectroscopy: Theory, experiment, and applications" *John Wiley & Sons*, 2018.

[19] E. T. McAdams, J. Jossinet. "Problems in equivalent circuit modelling of the electrical properties of biological tissues" *Bioelectrochemistry and Bioenergetics* 40(2) (1996) 147-152.

[20] K. S. Cole. "Permeability and impermeability of cell membranes for ions" *Cold Spring Harbor Symposia on Quantitative Biology* 8 (1940) 110-122.

[21] E. T. McAdams, J. Jossinet, A. Lackermeier. "Modeling the 'constant phase angle' behaviour of biological tissues: Potential pitfalls" *Innovation et Technologie en Biologie et Medecine* 16(6) (1995) 661-670.

[22] A. Sadkowski. "On the ideal polarisability of electrodes displaying cpe-type capacitance dispersion" *Journal of Electroanalytical Chemistry* 481(2) (2000) 222-226.

[23] R. L. Magin. "Fractional calculus in bioengineering. Part 2" *Critical Reviews in Biomedical Engineering* 32(1) (2004) 105-193.

[24] V. Vorpérian. "Fast analytical techniques for electrical and electronic circuits" *Cambridge University Press*, 2002.

[25] I. Podlubny. "Fractional differential equations" *Academic Press*, 1999.

[26] F. Mainardi. "On some properties of the Mittag-Leffler function $E_\alpha(-t^\alpha)$, completely monotone for $t>0$ with $0<\alpha<1$" *Discrete and Continuous Dynamical Systems Series B* 19(7) (2014) 2267-2278.

Capítulo 3

Objetivos

3 Objetivos

La presente Tesis Doctoral tiene como objetivo general el estudio teórico y aplicación experimental de la técnica de interrupción de corriente para una monitorización rápida del estado fisiológico de tejidos biológicos de roedor.

A continuación, se exponen los objetivos específicos que se persiguen en el presente trabajo de investigación.

(i) Establecer a nivel teórico el método de interrupción de corriente (CIM) como herramienta para estimar los valores de los parámetros de circuitos eléctricos equivalentes (EECs) que describan el comportamiento eléctrico pasivo de tejidos biológicos. Se pretende modelar las propiedades capacitivas no ideales del tejido utilizando un elemento de fase constante (CPE).

(ii) Implementar el CIM para obtener los parámetros de EECs en tejidos *ex vivo* que presenten diferencias histológicas y de excitabilidad, tales como el hígado y el músculo estriado de roedor. El hígado es un ejemplo de tejido de alta homogeneidad celular y excitabilidad eléctrica baja, en oposición al músculo estriado que posee baja homogeneidad celular y alta excitabilidad eléctrica. Se pretende llevar a cabo un análisis histológico en muestras de ambos tejidos después de aplicar el CIM y también comparar los valores de los parámetros de los EECs obtenidos mediante el CIM con los obtenidos a partir de medidas de impedancia.

(iii) Evaluar la funcionalidad del CIM para la monitorización *in vivo* de tejidos excitables del sistema neuromuscular de rata, en particular de la médula espinal y el músculo estriado. Este objetivo supone un paso previo a analizar los usos potenciales del CIM en las lesiones de la médula espinal, tanto en lo referente a la recuperación funcional como en lo que atañe a la mejora técnica en el diagnóstico clínico del déficit sensitivo y motor en sí. Los resultados obtenidos podrían permitir optimizar el diseño de neuroprótesis implantables crónicamente y mejorar la bioseguridad y eficacia de los protocolos de estimulación eléctrica. También se pretende comparar los valores de los parámetros de los EECs obtenidos utilizando el CIM y medidas de impedancia.

(iv) Generalizar el método de inyección súbita de carga (método "culostático", CM) a un sistema electrodo/solución fisiológica/electrodo donde las propiedades capacitivas no ideales de la interfase electrodo/solución fisiológica se describan mediante un CPE. La solución fisiológica simula de manera muy simplificada el comportamiento eléctrico de un tejido biológico. Este objetivo supone un paso previo para la aplicación del CM en la obtención de EECs en tejidos, lo que permitiría un menor riesgo de lesión por la reducción del tiempo de exposición del tejido a la corriente.

Capítulo 4

Discusión conjunta y artículos publicados

4 Discusión conjunta y artículos publicados

A continuación se lleva a cabo una discusión conjunta de los tres artículos publicados y que se incluyen en el presente Capítulo.

4.1 Discusión conjunta

En esta Tesis Doctoral se implementa la técnica de interrupción de corriente (CIM) para la estimación en tiempo real de los parámetros de un circuito eléctrico equivalente (EEC) de de Fricke y Morse generalizado, en el que las propiedades capacitivas del tejido se modelan utilizando un elemento de fase constante (CPE). Utilizando el CIM y también medidas de impedancia se ha estudiado el comportamiento eléctrico pasivo de tejidos excitables y no excitables de roedor, tanto *ex vivo* (tejidos extraídos del animal después de la perfusión y el sacrificio) como *in vivo* (con el animal anestesiado). Los valores de los parámetros de los EECs obtenidos se corroboraron utilizando la técnica convencional de medidas de impedancia. También se llevó a cabo un análisis histológico de los tejidos ensayados *ex vivo* para mostrar que el CIM no produjo daño adicional.

En primer lugar, el CIM se utilizó para obtener los EECs de hígado y músculo estriado de roedor. Ambos tejidos se seleccionan por sus diferencias histológicas y de excitabilidad. El hígado es un ejemplo de tejido de alta homogeneidad celular y excitabilidad eléctrica baja, en oposición al músculo estriado que presenta baja homogeneidad celular y alta excitabilidad eléctrica. Posteriormente se obtuvieron *in vivo* los EECs que modelan el comportamiento eléctrico pasivo de los tejidos excitables del sistema neuromuscular de rata, específicamente de la médula espinal y del músculo tríceps sural. Un análisis estadístico de los valores de los parámetros de los EECs permitió dilucidar su significado fisiológico. Por último, como un paso previo a una exposición más corta del tejido a la corriente (antes de su interrupción) y utilizando un CPE se ha generalizado el método de inyección súbita de carga (método "culostático", CM) en un sistema "platino/solución fisiológica tampón fosfato salino (PBS)/platino". La solución de PBS constituye un simulador muy simplificado de las propiedades eléctricas de tejidos biológicos.

La técnica de interrupción de corriente (CIM) es una herramienta fidedigna para la monitorización en tiempo real, tanto *ex vivo* como *in vivo*, de tejidos biológicos a través de sus EECs. Una fortaleza del CIM es su interpretación física clara ya que dado el carácter multidisciplinar de las ciencias biológicas modernas, permite buscar correlaciones con parámetros anatómicos, bioquímicos y moleculares ya conocidos y establecer criterios para su aplicación.

Además, en el contexto de las neuroprótesis, los resultados que se muestran son de interés puesto que los dispositivos capaces de evocar respuestas motoras complejas diseñadas para pacientes con enfermedades neurológicas tendrán que actuar tanto sobre el sistema nervioso central (CNS) como sobre los músculos efectores. La combinación de la adquisición de datos a alta velocidad, a partir de medidas eléctricas basadas en la carga y descarga de las membranas celulares, y el conocimiento de las propiedades eléctricas específicas y

diferenciales de estos tejidos podría ayudar a optimizar el diseño de las neuroprótesis implantables crónicamente y los protocolos de estimulación eléctrica.

Aunque el CIM es capaz de describir estados tisulares complejos, lo cual es de utilidad en aplicaciones clínicas, es necesario adaptarlo a modelos eléctricos más complicados para que su respuesta teórica describa fielmente los resultados experimentales obtenidos desde dichos estados tisulares.

4.2 Artículos publicados

A continuación, se indican los artículos a los que ha dado lugar la presente Tesis Doctoral. Todos ellos han sido publicados en revistas incluidas en el *Science Citation Index*.

1. E. Hernández-Balaguera, E. López-Dolado, J. L. Polo. "Obtaining electrical equivalent circuits of biological tissues using current interruption method, circuit theory and fractional calculus" *RSC Advances* 6 (2016) 22312-22319.

2. E. Hernández-Balaguera, E. López-Dolado, J. L. Polo. "*In vivo* rat spinal cord and striated muscle monitoring using the current interruption method and bioimpedance measurements" *Journal of the Electrochemical Society* 165(12) (2018) G3099-G3103.

3. E. Hernández-Balaguera, J. L. Polo. "A generalized procedure for the coulostatic method using a constant phase element" *Electrochimica Acta* 233 (2017) 167-172.

4.2.1 Artículo nº 1

Autores: E. Hernández-Balaguera, E. López-Dolado, J. L. Polo
Título: Obtaining electrical equivalent circuits of biological tissues using current interruption method, circuit theory and fractional calculus
Revista: RSC Advances
Volumen: 6
Páginas: 22312-22319
Año: 2016
Web: http://pubs.rsc.org/en/content/articlelanding/2016/ra/c5ra24535d

Abstract

We have adapted the current interruption method to obtain electrical equivalent circuits of rat tissues (liver viscera and triceps surae muscle). The paper provides a comprehensive and in-depth explanation of the procedure and its suitability has been assessed. Experimental data are interpreted using circuit theory and fractional calculus. A histological analysis was also carried out. The technique proposed has a clear physical meaning and we have tried to make this communication accessible to the potential readers with multidisciplinary backgrounds. To the authors' knowledge, there is no previous report of adapting the current interruption method to obtain electrical equivalent circuits of tissues using a four-electrode arrangement, circuit theory and fractional calculus.

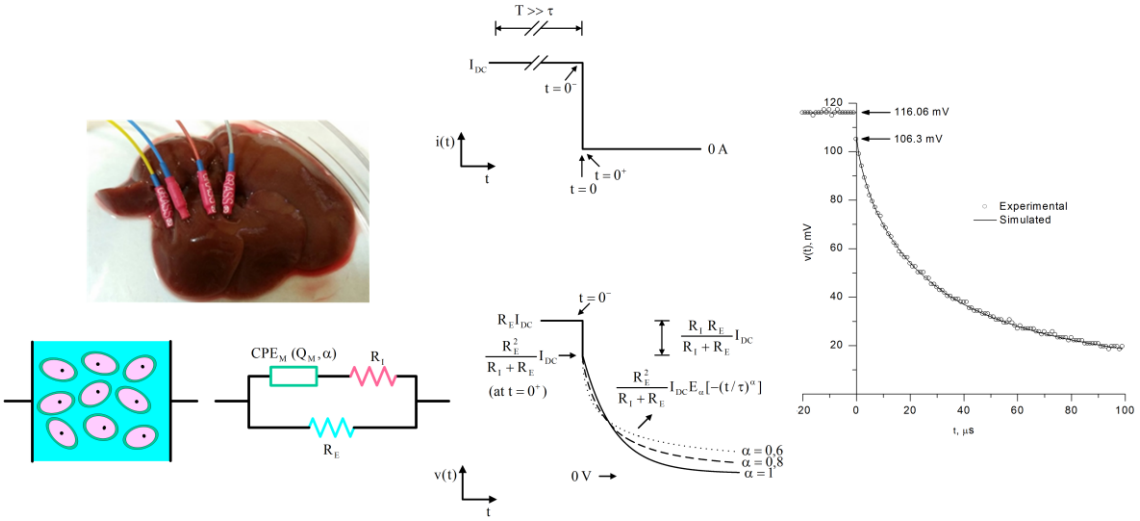

Keywords: Bioimpedance measurements, current interruption method, fractional calculus, biological tissues, time domain, impedance spectroscopy, electrical equivalent circuit.

1. Introduction

Impedance Spectroscopy (IS) is a well-established technique used in determining the physiological state of biological tissues from their electrical properties,[1,2] which involve the electrochemical processes for the intracellular-space/cell-membrane/extracellular-space system. In this introduction we review succinctly some basic concepts which will serve to expose the reader to the current interruption method for the electrical characterization of tissues.

Fig. 1(A) shows a schematic of single eukaryotic cell. Intracellular (pink color) and extracellular (blue color) spaces are electrolyte solutions containing primarily Na^+, K^+ and Cl^-. Cell membrane (green color), about 7 nm thick, separates intra- and extracellular compartments regulating the ionic concentration differences (cellular homeostasis).[2]

Let us consider an electric current flowing from left to right through the single cell of Fig. 1(A). In general, a portion of this current will cross the cell membrane and will enter the intracellular fluid. The remaining current will flow through extracellular fluid. Both current paths are implemented in the electrical equivalent circuit (EEC) of Fig. 1(B) using two parallel branches. The upper branch (capacitance C_M in series with a resistance R_I) models the current path through the cell membrane and the intracellular space. The lower branch (resistance R_E) considers the current path through the extracellular compartment. Note that cell membrane acts as an electrical capacitor by involving a charge separation. Intra- and extracellular environments (electrolyte solutions) are represented by the intra- and extracellular resistances, R_I and R_E, respectively. EEC of Fig. 1(B) was initially proposed by Fricke and Morse.[3]

Fig. 1(C) shows a portion of tissue which involves a group of similar cells. Thus, the EEC of Fig. 1(D) comprises an array of interconnected EECs (each EEC corresponds to a single cell) which provides a modified Fricke and Morse EEC. The capacitor C_M is replaced by a fractional capacitor,[4] or more generally known as constant phase element (CPE_M) where Q_M and α are the CPE_M parameters (see below). [2,5] CPE_M takes into account the space distribution of the electrical tissue properties. While the EEC of Fig. 1(B) exhibits one single time-constant, the EEC shown in Fig. 1(D) involves a distribution of time constants.

Fig. 1(E) redraws the EEC of Fig 1(D). i(t) is the current supplied to the circuit (excitation). Currents and voltages have been labeled in each element. $i_M(t)$ and $i_E(t)$ are the currents through the CPE_M and R_E, respectively. $v_M(t)$, $v_I(t)$ and $v_E(t)$ are the voltages across the CPE_M, R_I, and R_E, respectively. Eq. (1) expresses $i_M(t)$ as a function of $v_M(t)$,

$$i_M(t)=Q_M\frac{d^\alpha v_M(t)}{dt^\alpha} \qquad (1)$$

where Q_M has the units of (farads)×(seconds)$^{\alpha-1}$ with v(t) in volts, $i_M(t)$ in amperes and t in seconds. α is a dimensionless quantity $0<\alpha<1$. d^α/dt^α is the fractional-order derivative of order α. If we let $\alpha=1$, Eq. (1) involves a ordinary derivative and CPE_M is an ideal capacitor ($Q_M=C_M$).[4]

It is important to point out that the CPE_M and the resistors R_I and R_E are LTI (linear time-invariant) circuit elements. Indeed, the parameters Q_M, α, R_I, and R_E do not vary with

time (time-invariant property) and do not depend on voltages across and/or currents through the corresponding circuit element under consideration (linear property). It follows that the EEC of Fig 1(E) is a LTI circuit.[6]

Fig. 1(F) shows the EEC of Fig. 1(E) transformed into the frequency-domain which is usually used in IS. Thus, $i(t)$, $i_M(t)$, $i_E(t)$, $v_M(t)$, $v_I(t)$, and $v_E(t)$ are replaced by their corresponding phasors $\bar{I}$, $\bar{I}_M$, $\bar{I}_E$, $\bar{V}_M$, $\bar{V}_I$, and $\bar{V}_E$, respectively. The impedances of the circuit elements, $Z_{CPE_M}(j\omega)$, R_I, and R_E, are also indicated.

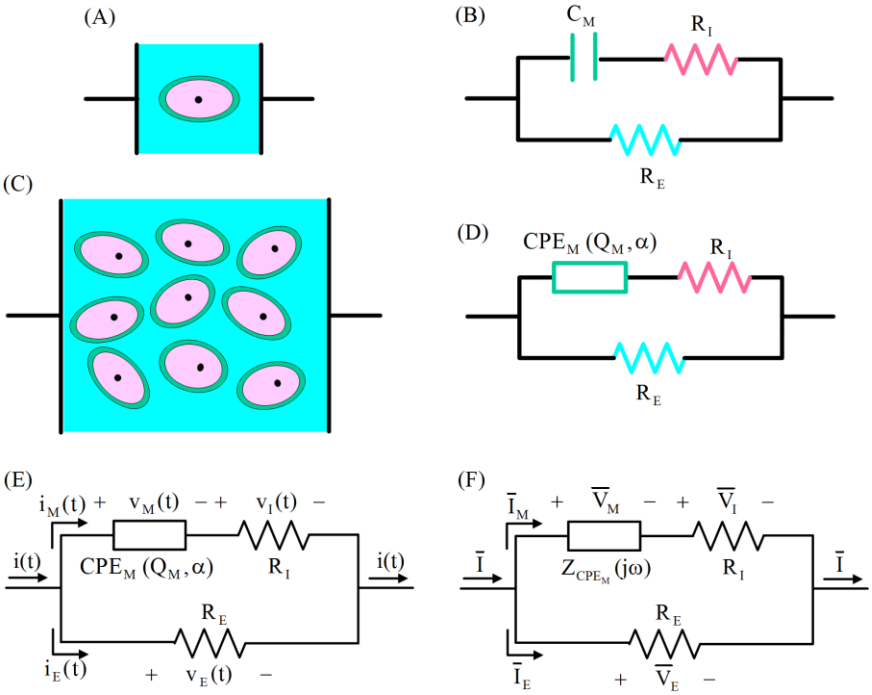

Figure 1. Cell, tissue and electrical equivalent circuit (EEC). (A) Single eukaryotic cell. (B) EEC of the cell shown in Fig. 1(A). (C) Biological tissue. (D) EEC of the tissue shown in Fig. 1(C). (E) EEC of Fig. 1(D) in the time domain and (F) frequency domain.

Specifically, the impedance of the CPE_M (ratio $\bar{V}_M/\bar{I}_M$) is written as[5]

$$Z_{CPE_M}(j\omega)=\frac{1}{Q_M(j\omega)^{\alpha}} \tag{2}$$

where ω is the angular frequency ($\omega=2\pi f$ where f is frequency) and j is the imaginary unit.

From Eqs. (1) and (2), we observe how the α fractional-order time derivative of a sinusoidal waveform is equivalent to multiplying the corresponding phasor by $(j\omega)^{\alpha}$.

The total impedance between the endpoints of the EEC of Fig. 1(F) is found be

$$Z(j\omega)=\frac{R_I R_E}{R_I+R_E}+\frac{R_E-\frac{R_I R_E}{R_I+R_E}}{1+\left[j\omega\left[\left(R_I+R_E\right)Q_M\right]^{\frac{1}{\alpha}}\right]^{\alpha}} \tag{3}$$

In Eq. (3), we find that the coefficient of (jω) -physical frequencies- is the distributed time-constant (τ) of the EEC of Fig. 1(E) when a current is supplied to it; that is,

$$\tau=[(R_I+R_E)Q_M]^{\frac{1}{\alpha}} \tag{4}$$

Observe that if α=1 (CPE_M is an ideal capacitor), Eq. (3) yields the impedance of the EEC of Fig. 1(B) and its time constant is written as $(R_I+R_E)C_M$ where (R_I+R_E) is the resistance seen by C_M (a current source is replaced by an open circuit). The inverse of the time constant provides the characteristic frequency ω_o (known as frequency pole in first-order (α=1) LTI circuits)[7]

$$\omega_o=\tau^{-1}=[(R_I+R_E)Q_M]^{-\frac{1}{\alpha}} \tag{5}$$

It is worth remembering that impedance Z(jω) is a complex number whose real and imaginary parts are the resistance R(ω) and the reactance X(ω), respectively. That is, Z(jω)=R(ω)+jX(ω). Note that at sufficiently low and high frequencies, Eq. (3) yields approximately R_E and $R_IR_E/(R_I+R_E)$, respectively. The same conclusion can be stated from the EEC of Fig. 1(F). Suppose that a sinusoidal current i(t) is connected to the EEC of Fig. 1(E) and a sinusoidal steady-state is reached (refer to Fig. 1(F)). At sufficiently low frequencies, the impedance magnitude of the upper branch $|Z_{CPE_M}(j\omega)+R_I|$, will become large enough to cause $|Z_{CPE_M}(j\omega)+R_I| \gg R_E$, so almost all the current i(t) will flow through the extracellular space (resistor R_E), resulting in $i_E(t)\sim i(t)$. At sufficiently high frequencies, $R_I \gg |Z_{CPE_M}(j\omega)|$, the current will flow through both intra- and extracellular media according to the current-divider rule (circuit consisting of R_I and R_E).

Interestingly, the expression in Eq. (3) is of the same form as that proposed by Cole[8]

$$Z(j\omega)=R_\infty+\frac{R_0-R_\infty}{1+(j\omega\tau)^\alpha} \tag{6}$$

where the high- and low-frequency limit resistances are $R_\infty=R_IR_E/(R_I+R_E)$ and $R_0=R_E$, respectively. The four parameters R_∞, R_0, τ (or ω_0) and α are known as Cole parameters.

Of specific interest in IS the Nyquist plot (-X(ω) vs. R(ω) in the complex plane). Nyquist plot of Eq. (3) sketches a depressed semicircle (the center of its corresponding circle lies below the real axis).[1,2] This depressed semicircle intersects the real axis at two points: $R_IR_E/(R_I+R_E)$ and R_E at the frequencies $\omega\to\infty$ and ω=0, respectively (see above).

It is easy and intuitive to see that changes in a biological tissue will be reflected in the corresponding EEC. For instance, consider an ischemic tissue. Cell swelling causes a reduction of the extracellular volume which yields an increase of the extracellular resistance R_E in the EEC of Fig. 1(D).[9] Next, to determine the parameters of the EEC shown in Fig. 1(D), electrical measurements are taken on the tissue under study.

One simple way of obtaining the electrical properties of biological tissues is using the four-electrode or Kelvin method,[1,2] as shown in Fig. 2(A). Four electrodes are placed into the tissue in a straight line. An electric current i(t) is injected from electrode 1 (EL1) and

collected at electrode (EL4). It determines a potential distribution in the tissue, resulting in a voltage v(t) between the two inner electrodes (EL2 and EL3). This setup (voltage-measuring electrodes placed in line and between the current-injecting electrodes) may usually provide a good signal to noise ratio. Fig. 2(B) shows the EEC of the four-electrode method. EEC_{ELi} and $EEC_{ELi/T}$ are the electrical equivalent circuits of the electrode i and (electrode i)/(surrounding tissue) interface, repectively. EEC_{Tij} is the equivalent circuit of the tissue portion carrying the current i(t) and placed between the two equipotential surfaces (perpendicular to current flow lines) which contain the electrodes i and j. Note that in circuit theory, we find voltages and currents which can also be measured using voltmeters and ammeters. Nevertheless, field theory should be regarded if we want to analyze the potential or current distributions in tissue or in the electrode/tissue interface.[10]

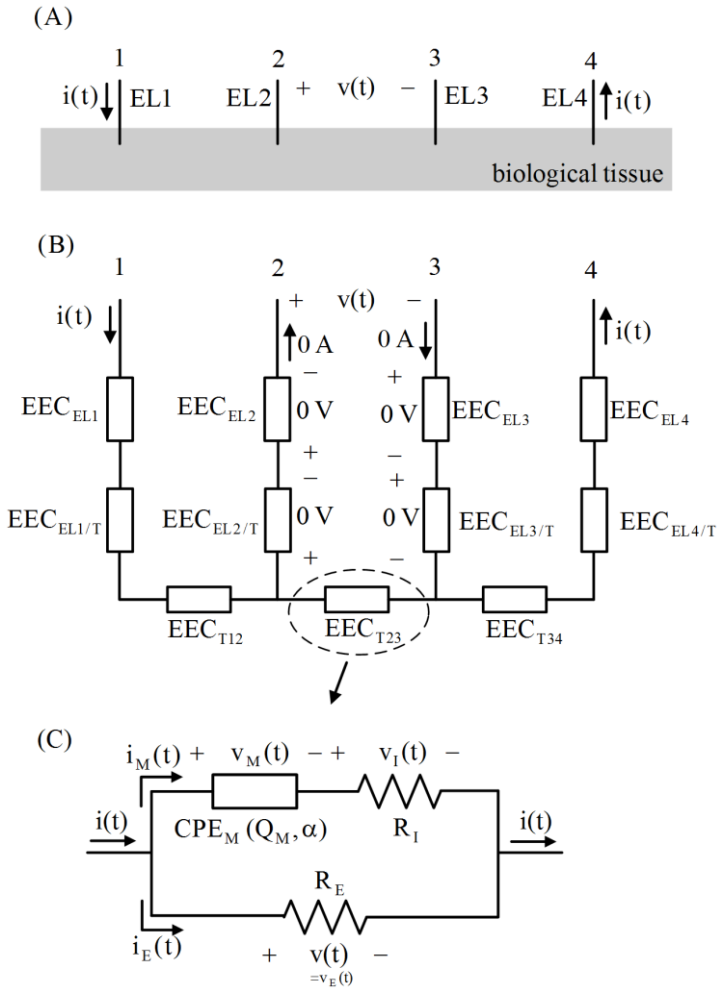

Figure 2. Four-electrode method. (A) Four electrodes are placed into the tissue. (B) EEC of the four-electrode arrangement shown in Fig. 2(A). (C) EEC of the tissue portion which is measured using the four-electrode method.

Simple EECs of EL_i and EL_i/T interface comprise a resistor and a capacitor (or CPE) in parallel with a resistor, respectively. Electrodes may also involve more complex processes such as anomalous diffusion.[11] Typical EEC_{Tij} is shown in Fig. 1(D). Note that in sinusoidal steady-state analysis, EEC_{ELi}, $EEC_{ELi/T}$, and EEC_{Tij} are replaced by their corresponding impedances $Z_{ELi}(j\omega)$, $Z_{ELi/T}(j\omega)$, and $Z_{Tij}(j\omega)$, respectively.

Since an ideal voltage-measuring device draws no current (open circuit), it follows from Fig. 2(B) that the measured voltage v(t) between terminal 2 and terminal 3 is equal as that of EEC_{T23}. This makes the four-electrode method suitable for characterizing the average electrical properties of the tissue portion which carries the current i(t) and contributes to the voltage v(t) between terminals 2 and 3. Fig. 2(C) shows the EEC_{T23} of the tissue portion which is measured. Note that the measured voltage v(t) is indeed the voltage $v_E(t)$ across the extracellular space (resistance R_E). We shall henceforth use $v_E(t)$ and v(t) interchangeably. Ideally, v(t) does not take into account the effects of electrode polarization (voltages across $EEC_{ELi/T}$). Errors in four-electrode configuration have been analyzed elsewhere.[12] Note that Fig. 1(E) is repeated here in Fig. 2(C) for the reader's convenience.

As the integrity of the cell membrane is a critical point to maintain the cell's life, the question arises as to what frequency range should be used to characterize its electrical properties. Cellular structure of tissues exhibits a characteristic frequency, $\omega_o/(2\pi)$, ranging from several kHz up to MHz. That range is known as β dispersion.[13,14] Thus, if a specific tissue has a characteristic frequency $\omega_o/(2\pi)$, an ideal situation is to cover an useful frequency range on both sides of ω_o to obtain accurate values for the parameters of the EEC. It should be pointed out that the tissues also exhibit other characteristic frequencies (α or γ dispersions) corresponding to different relaxation processes which may be evidenced in an impedance spectrum.[13,14]

We use entirely the LTI circuit theory.[6] Hence, the i(t)-v(t) relationship for the tissue (see Fig. 2(A)) should be described by a linear differential equation with constant coefficients. Although values of current, electric field or voltage have been proposed to ensure linear condition, they result in a large variability depending on the type of tissue and its state.[13-15] Additionally, the properties of a biological tissue can vary with time (for instance, during an ischemic event) and, thus, the measurement acquisition time should be sufficiently short to assure that the tissue is "frozen" in time (the electrical properties of the tissue do not change during the measurement acquisition time). This requirement is very critical for some processes such as electroporation.[15]

An important consideration is the current waveform i(t) to be injected. Characteristic current values should be sufficiently small to ensure the linearity (see above) but sufficiently large to allow an acceptable signal to noise relation without inflicting damage to the tissue (heating, pH changes or accumulation of toxic electrochemical products). The current density (the current per unit area) distribution in the tissue should be adequate to not inflict damage.[10]

Typically, experimental impedance measurements are obtained in a sequential way: Impedance at each frequency is measured using a single sinusoidal-signal which may be time-consuming. The use of excitation signals different from that sinusoidal-signal for analyzing electrical properties of tissue has been barely reported in the scientific literature.[15-20] Some advantages such as a drastic reduction of the measurement acquisition time and/or an optimum frequency spectrum which contains sinusoidal components of interest were emphasized.[17]

EECs of biological tissues have been obtained from the experimental transient-response to a step function.[19,20] Basically, a step excitation corresponds to a switch which closes at a specific instant and connects a dc battery to a given circuit.[6] For instance, the body composition was obtained from a step-voltage response using the two-electrode method.[19] Cole

parameters were determined in apple samples using a step-current response, fractional calculus, and also the two-electrode arrangement.[20]

In this paper, we have obtained EECs of rat tissues using the current interruption method (see below) which has a clear physical meaning. Cell membranes are constant current charged. When the current is cut-off, cell membranes begin to discharge through the surrounding intra/extracellular spaces. The analysis of the discharge voltage curve involves circuit theory and fractional calculus. Importantly, this discharge voltage curve depends only on the tissue's electrical properties.

The current interruption method has been used in electrochemistry to estimate ohmic losses.[21] We have adapted this method for obtaining the parameter values of the EEC shown in Fig. 1(D) using a four-electrode arrangement.

2. Current interruption method using a four-electrode arrangement

At this point, we explain the current interruption method and how the values for R_E, R_I, α, and Q_M are found. Figs. 3(A) and 3(B) show the waveforms of the current i(t) injected into the tissue and the resulting extracellular voltage v(t), respectively (refer to Fig. 2(A)).

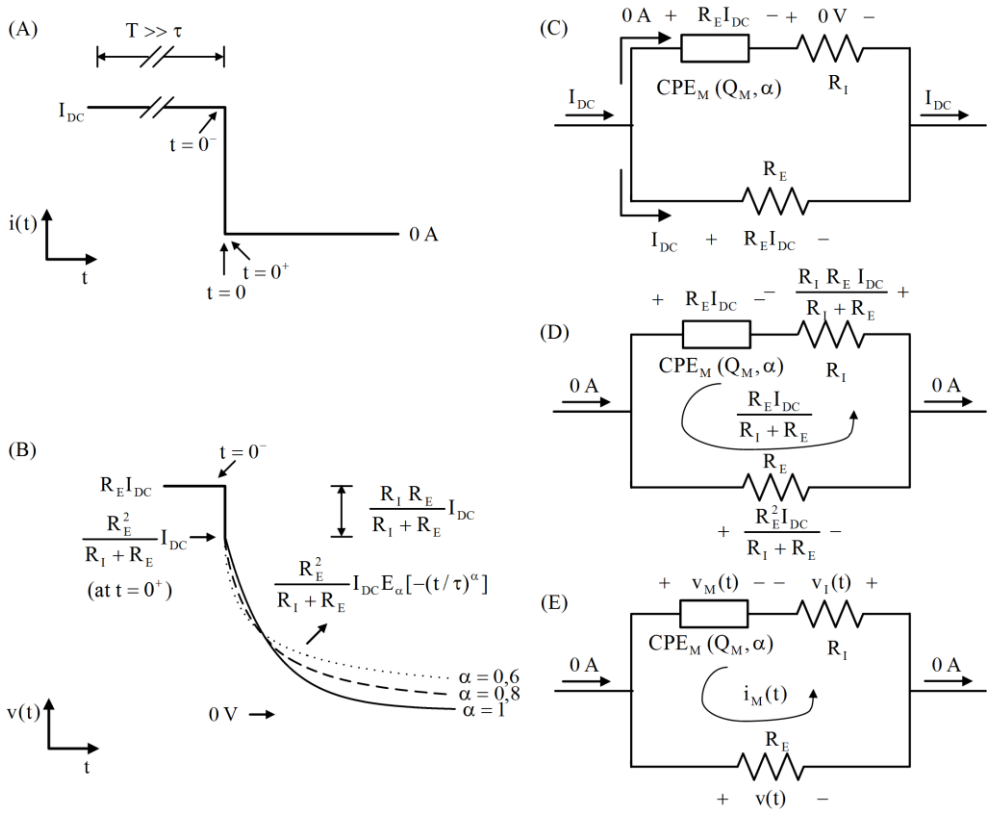

Figure 3. Current interruption method. (A) Waveform of the current injected into the tissue. (B) Waveform of the resulting extracellular voltage. (C) EEC of Fig. 1(E) at $t=0^-$. (D) EEC of Fig. 1(E) at $t=0^+$. (E) EEC of Fig. 1(E) for $t>0$.

Firstly, a dc current I_{DC} (excitation) is injected into the tissue between the two outer electrodes for a sufficiently long time T ($T>>\tau$, see below), so that the voltage (response)

between the two inner electrodes reaches a steady state (constant value). At time t=0, the current is abruptly cut off. Fig. 3(C) shows the EEC of Fig. 1(E) at $t=0^-$ (just before the current is interrupted). CPE_M is considered to be fully charged (dc steady-state) and acts as an open circuit. Thus all the current I_{DC} flows through the extracellular space (resistor R_E), yielding a voltage drop of $R_E I_{DC}$. Since no current flows through the cell membrane (upper branch), no voltage appears across the intracellular space (resistor R_I). It follows that the voltages across CPE_M and R_E are equal. Voltages and currents at $t=0^-$ are indicated on the circuit diagram in Fig. 3(C).

Just after interrupting the current (that is, at $t=0^+$), the energy previously stored in the cell membranes (CPE_M) begins to be released and dissipated in the surrounding intra/extracellular spaces. Fig. 3(D) shows the EEC of Fig. 1(E) at $t=0^+$. It is assumed that the voltage across the CPE_M cannot change instantaneously, so that the voltage across it just before ($t=0^-$) and just after ($t=0^+$) interrupting the current are equal. At $t=0^+$, the CPE_M voltage drives a current $R_E I_{DC}/(R_I+R_E)$ through R_E and R_I resistors, giving voltages of $R_E^2 I_{DC}/(R_I+R_E)$ and $R_I R_E I_{DC}/(R_I+R_E)$, respectively (refer to Fig. 3(D)).

Next, the voltage relaxation (free or natural response) is measured for t>0. Importantly, the natural response obtained for t>0 depends only on the tissue's electrical properties. Fig. 3(E) shows the EEC of Fig. 1(E) for t>0. Let us consider that CPE_M is an ideal capacitor ($\alpha=1$ and $Q_M=C_M$). From circuit theory, it can be shown that the expression for v(t) is written as $v(t)=[R_E^2 I_{DC}/(R_I+R_E)]e^{-t/\tau}$, where the time constant τ is $(R_I+R_E)C_M$ which is as that of Eq. (4) with $\alpha=1$ and $Q_M=C_M$. Nevertheless, CPE_M involves a fractional derivative -see Eq. (1)- and the Mittag-Leffler function is used to include a fractional relaxation.

$$v(t)=\frac{R_E^2}{R_I+R_E} I_{DC}\, E_\alpha\left[-\left(\frac{t}{\tau}\right)^\alpha\right] \tag{7}$$

where $E_\alpha(z)$ is the one-parameter Mittag-Leffler function,[22] defined as

$$E_\alpha(z)=\sum_{k=0}^{\infty}\frac{z^k}{\Gamma(\alpha k+1)} \tag{8}$$

Note that if $\alpha=1$, Eq. (8) is the Maclaurin series for the exponential function, resulting in $E_1(-t/\tau)=e^{-t/\tau}$.

The theoretically predicted waveform of v(t) has been sketched and clearly labeled in Fig. 3(B). Note that $R_I R_E I_{DC}/(R_I+R_E)$ is the magnitude of the jump discontinuity at t=0. Fig. 3(B) also shows that the fractional relaxation (Eq. (7)) exhibits a faster (slower) decay than the exponential one, for short (large) times.

The values of the parameters of the EEC shown in Fig. 1(D) are determined by performing the following procedure:

(i) R_E is found from the previous steady-state (value $v(0^-)$) as

$$R_E=\frac{v(0^-)}{I_{DC}} \tag{9}$$

(ii) R_I is obtained from the value of $v(0^+)$ as

$$R_I = \frac{R_E^2 I_{DC} - R_E v(0^+)}{v(0^+)} \tag{10}$$

(iii) The transient-voltage response is fitted to Eq. (7); α and τ are then determined. Finally, Q_M is calculated using Eq. (4). The fitting procedure was performed using a routine in MATLAB.[23]

We have assumed that the current is interrupted instantaneously (from $t=0^-$ to $t=0^+$). Nevertheless a finite (nonzero) fall time (t_f) exists in a real-life setup. The tissue will "feel" that the current is abruptly set to zero if $t_f << \tau$. It should also be noted that a transient recorder with a sufficiently sampling rate is needed in order to more accurately determine the critical points (jump discontinuity and the initial fast decay of the fractional relaxation) of the experimental waveform of v(t).

3. Experimental

Adult male Wistar rats were provided by a commercial supplier (Harlan Ibérica, Spain) and used at the age of *ca.* 25 weeks (n=3, 351±43 g). All experimental protocols adhered to the regulations of the European Commission (directives 2010/63/EU and 86/609/EEC) and the Spanish Government (RD53/2013) for the protection of animals used for scientific purposes. All the experiments were made at a room temperature.

Surgical procedures of organ and muscle extraction were performed under intraperitoneal (IP) analgesia with xylazine (10 mg/kg) and anesthesia with sodium pentobarbital (55 mg/kg) mixed with atropine (0.05 mg/kg). Eyes were covered with Lubrithal™ gel to prevent corneal abrasion and dehydration. In all cases, extreme care was taken to minimize muscle tissue damage. When deeply anesthetized, the skin and muscles over the breastbone were cut and the sternal manubrium was grasped to gain access to the thoracoabdominal union. The abdominal cavity was opened by cutting through the abdominal wall in the midline from the tip of the *processus xiphoideus* to the *pecten ossis pubis*. The liver was removed and imbibed in saline solution. After that, a right Achilles tenotomy was performed; the triceps surae was dissected, removed and immersed in saline solution just prior to carry out the electrical measurements. Rats were sacrificed immediately after the liver and triceps surae extraction with an IP lethal dose of sodium pentobarbital (110 mg/kg). Finally, organs were carefully examined looking for any findings of gross damage and properly prepared for subsequent electrical characterization.

We analyzed three samples of livers and other three of triceps surae muscles from three rats. Electrical measurements were taken on each sample using the current interruption method. Just after that, conventional bioimpedance measurements were obtained. This protocol is then repeated twice more in each one of the livers and muscles, to guarantee the reproducibility and repeatability of experimental data. We selected these two particular tissues because of their opposite characteristics related to cellular homogeneity and electrical excitability. So, we chose the liver as an example of high degree of cellular homogeneity but bad electrical excitability and the striated muscle (triceps surae), as an example of low degree of cellular homogeneity but good electrical excitability.

Electrical measurements were performed using four platinum needle electrodes. Each electrode (refer to Fig. 4(A)) was 10 mm long and 0.3 mm in diameter (Grass Technologies, subdermal needle electrode, model F-E2-48). The electrodes were placed into the tissue in a straight line and equally spaced (5 mm). Figs. 4(B) and 4(C) show the four-electrode arrangement for liver and triceps surae, respectively.

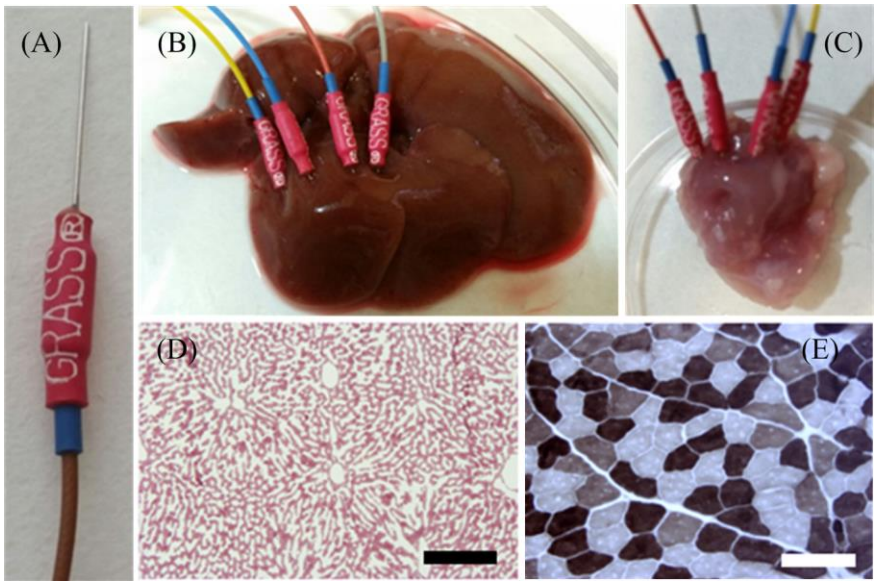

Figure 4. Four-electrode setup. (A) Platinum needle electrode. (B) Four platinum needle electrodes are placed into the liver and (C) into the triceps surae. (D) Representative 10x optical microscopy images of the liver after hematoxylin-van Gieson staining, showing a normal tissue structure. Black scale bar=100 μm. (E) Representative 40x transverse section of triceps surae muscle after ATPase staining, showing the normal aspect of the three types of muscle fibers: 1 (black ones); 2A (white ones); and 2B (gray ones). White scale bar=100 μm.

An AutoLab PGSTAT302N Potentiostat/Galvanostat (EcoChemie), combined with the ADC10M module, was used to implement the current interruption method. The instrument was controlled by a computer and driven by NOVA software. A dc current of 100 μA was injected between the two outer electrodes for 1 ms and just after that, the current is abruptly switched off. The voltage between the two inner electrodes was recorded between 1 ms before and 100 or 50 μs after switching off the current. A sampling rate of 10 MHz was used.

A Solartron 1260 frequency response analyzer connected to a Solartron 1294 impedance interface system were used to obtain the impedance measurements. Both instruments were controlled by a computer and driven by SMaRT software. Sinusoidal signals of 100-μA amplitude were injected between the two outer electrodes. The frequency-values were logarithmically spaced (5 steps/decade) between 1 MHz and 1 kHz.

After making electrical measurements, all samples were placed in paraformaldehyde 4% at 4°C for immersion-fixation and later, three days more in sucrose (30% in phosphate buffered saline, PBS) at 4°C for cryo-protection. Tissue pieces were mounted on plastic containers, quick-frozen in Optimal Cutting Temperature compound (Tissue Tek, Hatfield, PA) and cut in transverse sections of 10 μm by using a Microm HM550 cryostat. Livers and muscles were initially examined using hematoxylin-van Gieson (Fig. 4(D)) and ATPase (Fig. 4(E)) stainings, respectively. Digital images were collected with a fluorescence Olympus BX51 microscope with 2x, 10x, 20x, and 40x objectives.

4. Results and discussion

No significant acute damage was observed in the organs microscopically evaluated. Neither alteration of normal tissue structure, nor signs of inflammation or necrosis were found in the analyzed sections of the livers (Fig. 4(D)) and muscles (Fig. 4(E)). Thus, the electrical measurements corresponded to normal rat tissues and importantly, the technique presented has not acutely damaged them.

Figs. 5(A) and 5(B) show the resulting voltage for the liver and triceps surae, respectively. The shape of the waveforms is similar to that predicted theoretically (refer to Fig. 3(B)), showing: (i) the previous steady state; (ii) the jump discontinuity. Values of $v(0^-)$ and $v(0^+)$ have been indicated by arrowheads; and (iii) the voltage relaxation for $t>0$. Simulated data are also shown in Figs. 5(A) and 5(B). There is an excellent agreement between the experimental and simulated data. Average errors of 0.46% and 0.62% were obtained for liver and triceps surae, respectively. The following function was used: $\frac{100}{N\, v_{exp}^{max}} \sum_i |v_{exp}(t_i) - v_{sim}(t_i)|$, where $v_{exp}(t_i)$ and $v_{sim}(t_i)$ are the experimental and simulated voltages at time t_i, respectively, v_{exp}^{max} is the maximum value of $v_{exp}(t_i)$, and N is the total number of points.

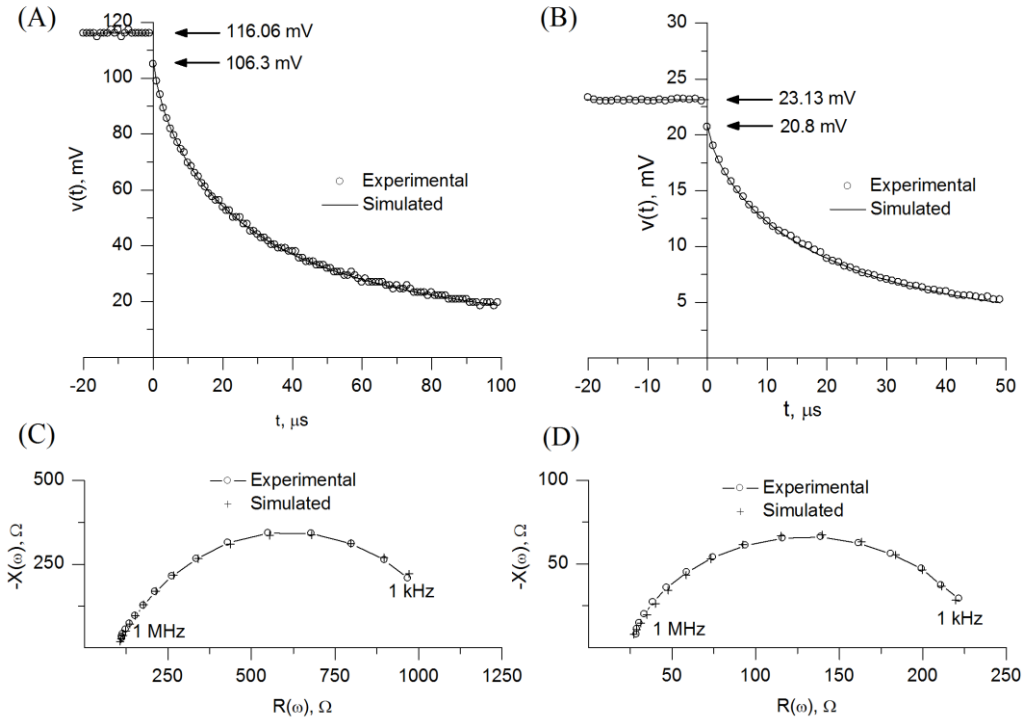

Figure 5. Experimental and simulated results. Waveforms of the resulting extracellular voltage for (A) the liver and (B) the triceps surae, using the current interruption method. Nyquist plots for (C) the liver and (D) the triceps surae.

Table 1 specifies the parameter values of the EEC shown in Fig. 1(D), using the current interruption method. They have been obtained by applying the procedure outlined in Section 2. Additionally, the values of the time constants associated with each of the two tissues have also been listed in Table 1.

Note that we should check whether end up with a consistent solution. The distributed time constants for the liver and triceps surae are about 30 μs and 20 μs, respectively. Thus we see that a previous steady state is reached because 1 ms >> 30 μs and 1 ms >> 20 μs. A sampling rate of 10 MHz allowed more accurate values for $v(0^-)$ and $v(0^+)$ and to measure the time taken for the experimental setup to change the current from the previous steady-state value to zero. This fall time (t_f) was of about 1 μs. Thus, the tissue "feels" that the current is abruptly switched off because 1 μs << 30 μs and 1 μs << 20 μs. For clarity's sake, only the samples taken every 1 μs are shown in Figs. 5(A) and 5(B). The previous steady state is shown during the 20 μs preceding the current interruption.

Table 1. Parameter values of the EEC shown in Fig. 1(D), obtained using the current interruption method and the conventional IS technique. Distributed time constants are also indicated.

Biological tissue	Measurement method	R_E (Ω)	R_I (Ω)	Q_M (nF $s^{\alpha-1}$)	α	τ (μs)
Liver Viscera	Current Interruption Method	1160.6	106.6	361.1	0.74	30.7
	Impedance Spectroscopy Measurements	1146.1	107.8	412.6	0.73	31.5
Triceps Surae Muscle	Current Interruption Method	231.3	25.9	1432.3	0.73	19.8
	Impedance Spectroscopy Measurements	238.7	25.3	1260.3	0.72	14.8

Typical Nyquist plots for the liver and triceps surae are shown in Figs. 5(C) and 5(D), respectively. Well defined depressed semicircles can be observed. Experimental impedance data were fitted to the EEC shown in Fig. 1(D) using ZView software. The parameter values obtained are listed in Table 1. Impedance plots also show simulated data which have been obtained using the EEC of Fig. 1(D) and the parameter values given in Table 1. As can be seen there is an excellent agreement between the experimental and simulated results. Average errors of 0.27% and 0.51% were obtained for liver and triceps surae, respectively. We have used the following expression: $\frac{100}{N\, Z_{exp}^{max}} \sum_i |Z_{exp}(j\omega_i) - Z_{sim}(j\omega_i)|$, where $Z_{exp}(j\omega_i)$ and $Z_{sim}(j\omega_i)$ are the experimental and simulated impedance data at the frequency ω_i, respectively, Z_{exp}^{max} is the maximum impedance magnitude of experimental data, and N is the total number of points. Note that the calculated average errors are normalized to the maximum value in the data set.[24]

Table 1 shows that the parameter values obtained using the current interruption method are remarkably close to those found from IS measurements. We note minor discrepancies of less than 3% for R_E, R_I, and α parameters and of the order of 10% for Q_M parameter. Determination of Q_M is more prone to errors because it depends on R_E, R_I, α, and τ. In turn, α and τ are obtained from the fitting procedure (see Section 2). Even so, a reasonable estimate for Q_M could be obtained.

The measurement acquisition time (1.1 ms and 1.05 ms for the liver and triceps surae, respectively) using the current interruption method is much shorter than that of the conventional impedance spectroscopy technique (~35 s). Thus, it may allow monitoring of fast

changes in a biological tissue. Nevertheless, as we have seen earlier, specific requirements on current interruption time and sampling rate should be fulfilled.

5. Conclusions

We have obtained EECs of rat tissues using the current interruption method and also impedance spectroscopy measurements (for comparative purposes). Accurate estimates of EEC parameters have been obtained using circuit theory and fractional calculus. Extra/intracellular resistances are obtained at time instants just before and just after interrupting the current. In order to determine the cell membrane parameters (CPE parameters), the transient-voltage response is fitted to the fractional relaxation equation. Importantly, this discharge voltage curve depends only on the tissue's electrical properties. Because of its ability to perform very fast measurements, this method (used here for the first time) may allow a real-time monitoring of the physiological state of tissues. Specific requirements on current interruption time and sampling rate have to be fulfilled. The histological images analysis showed that the technique presented did not produce acute damage to the tissues studied.

Acknowledgements

This work was funded by Junta de Comunidades de Castilla-La Mancha (Project PEII-2014-021-A). E. Hernández-Balaguera expresses his gratitude to the Universidad de Castilla-La Mancha for the Pre-PhD contract granted to him.

References

1 B. Rigaud, J. P. Morucci and N. Chauveau, *Crit. Rev. Biomed. Eng.*, 1996, **24**, 257-351.
2 S. Grimnes and O. G. Martinsen, *Bioimpedance and Bioelectricity Basics*, Academic Press, London, 2015.
3 H. Fricke and S. Morse, *J. Gen. Physiol.*, 1925, **9**, 153-167.
4 R. L. Magin, *Crit. Rev. Biomed. Eng.*, 2004, **32**, 105-193.
5 E. T. McAdams, J. Jossinet and A. Lackermeier, *Innov. Tech. Biol. Med.*, 1995, **16**, 662-670.
6 F. F. Kuo, *Network Analysis and Synthesis*, John Wiley & Sons, New York, 1966.
7 A. S. Sedra and K. C. Smith, *Microelectronic Circuits*, Oxford University Press, New York, 2004.
8 K. S. Cole, *Cold Spring Harbor Symp. Quant. Biol.*, 1940, **8**, 110-122.
9 E. Gersing, *Bioelectrochem. Bioenerg.,* 1998, **45**, 145-149.
10 G. R. Hernández-Labrado, J. L. Polo, E. López-Dolado and J. E. Collazos-Castro, *Med. Biol. Eng. Comput.*, 2011, **49**, 417-429.
11 G. R. Hernández-Labrado, R. E. Contreras-Donayre, J. E. Collazos-Castro and J. L. Polo, *J. Electroanal. Chem.*, 2011, **659**, 201-204.
12 S. Grimnes and O. G. Martinsen, *J. Phys. D: Appl. Phys.*, 2007, **40**, 9-14.
13 H. P. Schwan, *Adv. Biol. Med. Phys.*, 1957, **5**, 147-209.

14 H. P. Schwan, *Proceedings of 16th Annual International Conference of the IEEE Engineering in Medicine and Biology Society*, Baltimore (United States), 1994.
15 U. Pliquett, *Proceedings of the 11th International Biennial Baltic Electronics Conference*, Tallinn (Estonia), 2008.
16 U. Pliquett, E. Gersing and F. Pliquett, *Biomed. Tech.,* 2000, **45**, 6-13.
17 M. Min, U. Pliquett, T. Nacke, A. Barthel, P. Annus and R. Land, *Physiol. Meas.*, 2008, **29**, S185-S192.
18 U. Pliquett, *Proceedings of the XV International Conference on Electrical Bio-Impedance (ICEBI) & XIV Conference on Electrical Impedance Tomography (EIT)*, Heilbad Heiligenstadt (Germany), 2013.
19 C. E. B. Neves and M. N. Souza, *Physiol. Meas.*, 2000, **21**, 395-408.
20 T. J. Freeborn, B. Maundy and A. S. Elwakil, *Comput. Electron. Agric.*, 2013, **98**, 100-108.
21 F. H. van Heuveln, *J. Electrochem. Soc.*, 1994, **141**, 3423-3428.
22 I. Podlubny, *Fractional Differential Equations*, Academic Press, San Diego, 1999.
23 I. Podlubny, I. Petrás and T. Skovránek, *Proceedings of the 13th International Carpathian Control Conference* (ICCC 2012), High Tatras (Slovakia), 2012.
24 M. Urquidi-Macdonald, S. Real and D. D. Macdonald, *J. Electrochem. Soc.*, 1986, **133**, 2018-2024.

4.2.2 Artículo nº 2

Autores: E. Hernández-Balaguera, E. López-Dolado, J. L. Polo
Título: *In vivo* rat spinal cord and striated muscle monitoring using the current interruption method and bioimpedance measurements
Revista: Journal of the Electrochemical Society
Volumen: 165
Número: 12 (Focus Issue on the Brain and Electrochemistry)
Páginas: G3099-G3103
Año: 2018
Web: http://jes.ecsdl.org/content/165/12/G3099.full

Abstract

The therapeutic value of implantable neuroprosthetic devices would improve considerably if it were possible to monitor the electrical properties of the neural tissue, so that the stimuli to the nervous system can be optimally, efficiently and safely applied. The current interruption method (CIM) was previously described by the authors to obtain *ex vivo* electrical equivalent circuits (EECs) of rat liver and triceps surae (TS) tissues using a four-electrode arrangement, fractional calculus, and circuit theory. The aim of this paper was to investigate the use of CIM for *in vivo* real-time monitoring of rat spinal cord and striated muscle, as a prior step to addressing their potential uses in spinal cord injury or other conditions involving central nervous system (CNS) damage. Statistical analysis of the EEC parameter values was carried out to elucidate their physiological meaning and their possible uses in implantable neural prostheses.

One of the more promising approaches to restoring or improving lost functions after central nervous system (CNS) damage, is the use of chronically implanted electrodes inside the CNS to modulate the neural circuit responses. For this purpose, the neuroprostheses use electrodes that allow muscles, nerves, spinal cord or brain to be stimulated.[1] When an electrode is implanted chronically into the neural tissue, three distinct regions take part in the propagation of stimuli or in a biopotential measurement: (i) the electrode itself; (ii) the electrode/neural tissue interface; and (iii) the bulk neural tissue. Thus, an in depth knowledge of the electrical and electrochemical properties of each region is required for the design of optimal, efficacious and safe protocols of therapeutic value.[2]

The challenge regarding human neural interfaces consists in being able to record biopotentials and apply an appropriate stimulation protocol over the chronic timescales.[3] Much effort has been devoted to electrode materials aimed at a better biointegration into the surrounding tissue and improvement in the electrical properties of the electrode/neural tissue interface.[3-5] However, in the context of the implantable neuroprosthetics, no special attention has been paid to the electrical properties of the tissue itself and they are of great importance because, besides underlying its physiological state, they determine the propagation of the applied stimuli and consequently the therapeutic benefits. In general, the space distribution of the electrical tissue properties involves resistance (intra- and extra-cellular spaces) and capacitance (cell membrane separates the charge) leading to a frequency-dependent circuit, that is, a filter electrical circuit.[6] In addition, some experimental measurements have indicated that the complex environment (an electrolyte-rich solution consisting of high cell density and extra-cellular matrix materials, with complex paths) around neurons is also frequency dependent, which is a key point for the volume conduction of an electrical signal.[7,8] Thus, the stimulus signal (or an endogenously generated field) is filtered (frequency-weighted) while travelling from the place in which it is applied to the location of the target tissue.[9] An accurate electrical representation of the tissue itself would allow us to optimize the clinical stimulus waveforms.[10] Specifically, in voltage (or current) regulating devices, the waveform of the therapeutic current (or voltage between electrodes) changes due to variations of the tissue and electrode-tissue impedances because they are not pure resistances.[11]

Impedance Spectroscopy (IS) is a well-established technique which allows the electrical properties of the tissues to be determined by measuring their electrical impedance over a wide frequency range of interest (β dispersion).[12] In the literature, the electrical properties of the brain tissue itself (gray and white matters) have been described as a function of the frequency, in terms of dielectric properties[13,14] or impedance,[15,16] including *ex-* and *in-vivo* measurements. Although focused on the electrode-tissue impedance, other research has also considered the brain tissue component surrounding the electrode.[17,18] Conversely, the frequency-dependent electrical properties of the spinal cord have been very poorly studied in the literature. Recently, impedance measurements of *in vivo* ovine spinal cord tissue involving the electrode/pial surface were carried out in the context of optimizing spinal cord stimulation protocols.[19] However, a serious limitation is imposed by the sufficiently high conductivity of the cerebrospinal fluid (CSF) surrounding the neural tissue: the CSF shunts away most of the current that would have flowed through the tissue itself.[8,19,20]

Conventionally, bioimpedance measurements are obtained sequentially (a time-consuming process), that is, the electrical impedance at a specific frequency is obtained using a sinusoidal signal with the same frequency. For a drastic reduction of the measurement time, the current interruption method (CIM) was previously described by the authors

to obtain *ex vivo* electrical equivalent circuits (EECs) of rat liver and triceps surae (TS) tissues using a four-electrode arrangement, fractional calculus, and circuit theory.[6]

The circuit shown in Figure 1a represents the EEC of a biological tissue. It comprises a resistance R_E (extra-cellular medium) in parallel with the series combination of a resistance R_I (intra-cellular medium), and a constant phase element (CPE_M of parameters Q_M and α), which models the membrane's capacitive properties. The integrity of the cell membrane is critical to maintaining the cell's life. The parameters R_E and R_I vary slightly in normal conditions, but can be greatly modified in the presence of pathology (e.g., tissue inflammation due to trauma or infection will lead to extra-cellular edema and a consequent decrease in R_E).

Let a constant current I (see Figure 1b) be applied to the EEC of Figure 1a for a sufficiently long time (much greater than the time constant τ, with $\tau=[(R_E+R_I)Q_M]^{1/\alpha}$) and be abruptly interrupted at time t=0. The resulting voltage v(t) at the terminals of the EEC is sketched in Figure 1c.[6] At instant $t=0^-$ (just before the current is cut-off), $v(0^-)=R_E\times I$ which is the steady-state value. During the previous steady-state, CPE_M acts as an open circuit (no current flows through the cell membrane) and all the current flows through R_E: the extra-cellular space carries out all the current I as shown in Figure 1d. At instant t=0, I is cut-off (Figure 1b) and at $t=0^+$, immediately after interrupting I, the voltage is $v(0^+)=R_E^2I/(R_I+R_E)$. The jump discontinuity, $v(0^+)$-$v(0^-)$, as shown in Figure 1c, is due to the instantaneous resistive response of the extra- and intra-cellular media. Just after that (t>0), cell membranes discharge through the surrounding intra- and extra-cellular spaces (see Figure 1e), showing a fractional decay (Figure 1c) described by the one-parameter Mittag-Leffler function $E_\alpha[-(t/\tau)^\alpha]$. From an experimental transient-response v(t), the parameter values of the EEC of Figure 1a are obtained as follows: (i) R_E is found from the previous steady-state $v(0^-)$; (ii) R_I is calculated from the value of $v(0^+)$; (iii) α and τ are determined by fitting the experimental decay of v(t) to the expression $(R_E^2I/(R_I+R_E))\times E_\alpha[-(t/\tau)^\alpha]$ (refer to Figure 1c). Finally, Q_M is obtained from the value of τ.[6]

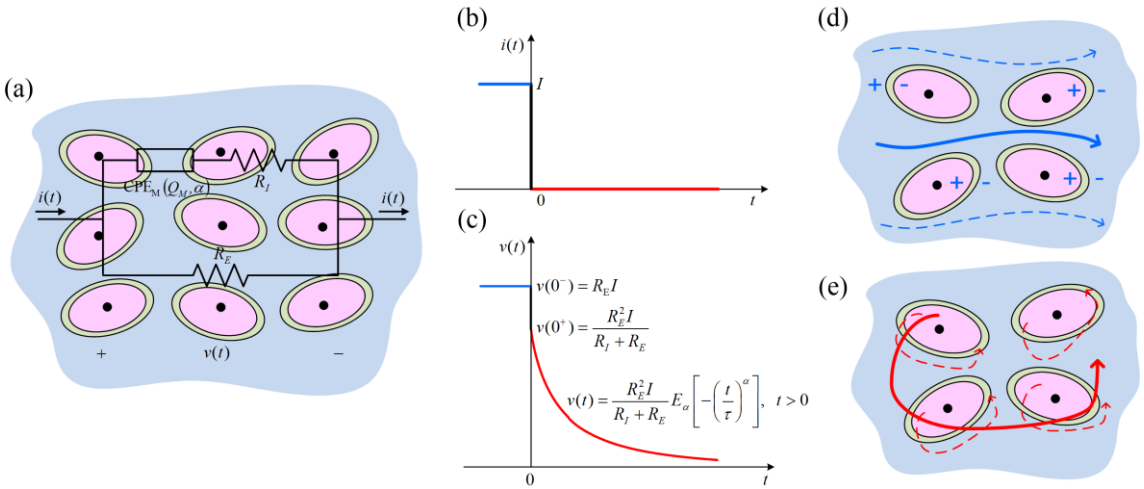

Figure 1. Current interruption method (CIM). (a) Electrical equivalent circuit (EEC) of the biological tissue, which involves a group of similar eukaryotic cells. Intra- and extra-cellular environments and cell membrane are shown in pink, blue, and green respectively. The black dots represent the cell nuclei. Waveform of the current injected into the tissue (b) and the transient-voltage response (c). Just before the electrical current is interrupted (at instant $t=0^-$), the cell membranes are fully charged and the electrical current flows through the extra-cellular space (d). Just after the current is cut-off (at instant $t=0^+$), cell membranes begin to discharge through the surrounding intra- and extra-cellular spaces (e).

The aim of this paper is to assess the CIM's effectiveness for *in vivo* real-time monitoring of the electrical properties of rat spinal cord and striated muscle, as a prior step to addressing their potential uses in spinal cord injury or other CNS damage conditions. Note that the final result of an implanted device for motor recovery will depend on the physiological states of both neural and effector muscle tissues. An EEC is obtained for both types of tissues. Finally, we carry out a statistical analysis of the parameter values of the EEC to elucidate their physiological meaning and their possible uses in implantable neural prostheses. For comparative purposes, conventional bioimpedance measurements were also obtained. We selected rat tissues because rodents are widely used as experimental animal models, and furthermore, both spinal cord and the striated muscles have been widely put to use as recipients of implantable neuroprostheses and/or regenerative devices to try to restore a number of human motor impairments.

Experimental

Surgical procedure. The experimental protocols adhered to the recommendations of the European Commission and the Spanish regulations for the protection of experimental animals (86/609/CEE, 32/2007, and 223/1988) and were approved by the Ethical Committee for Animal Research of the National Paraplegic Hospital of Toledo (Spain). Adult male Wistar rats (n=3, 16-24 weeks old, 380-500 g) raised at the hospital animal house facilities were used in this study. Previously, rats had been housed in groups of two with a 12 hour light/dark cycle with food and water available ad libitum. All surgical procedures were performed under general anesthesia with intraperitoneally applied sodium pentobarbital (55 mg/kg) mixed with atropine (0.02-0.2 mg/kg) and xylazine (10 mg/kg), administering a supplemental 30% of these drugs 90 min after the initial dose. An unguent was applied to the eyes to prevent pain from corneal abrasion. Animals were kept at 36 ºC with the aid of a thermal pad.

The back and neck of the anesthetized animals were shaved and disinfected with povidone iodine. A dorsal midline incision was made in the skin and superficial muscles of the neck region, and blunt dissection was carefully performed to expose the cervical spine. The vertebrae C4 to C6, which containing the spinal cord segment C5 to C7, were identified by counting from the vertebrae C2 and T2. The spinous apophysis and dorsal laminae of C4, C5 and C6 were removed without applying pressure on the underlying spinal cord. Subsequently, a transverse incision was performed in the dura mater, so that the dorsal part of the metameras was exposed and prepared for the intraspinal placement of the four electrodes to acquire the electrical measurements. Once the spinal cord records were completed, a new incision was made in the dorsal skin over the left hindpaw to expose the TS muscle, in which the four electrodes were placed to repeat the electrical measurements with a similar scheme to that followed for the spinal cord (see below). After finishing data acquisition, rats were immediately euthanized with an intraperitoneal lethal doses of pentobarbital.

Experimental protocol. Four-electrode setup consisted in four platinum needle electrodes (Grass Technologies, subdermal needle electrode, model F-E7: 10 mm long, 0.3 mm diameter) disposed in a straight line separated by an interelectrode distance of 4 mm, as shown in Figure 2a. Figures 2b and 2c illustrate the four-electrode arrangement placed into the rat spinal cord and striated muscle, respectively.

Figure 2. Experimental setup. (a) Four-electrode arrangement using 4 platinum needle electrodes. Four-electrode array is placed into the spinal cord (b) and the triceps surae (TS) muscle (c).

An AutoLab PGSTAT302N Potentiostat/Galvanostat (Eco-Chemie) was combined with the ADC10M module to implement the CIM. Under galvanostatic control, a dc current of 50 μA was injected between the two outer electrodes for a sufficiently long time (1 ms) and immediately afterwards, the current was abruptly interrupted (set to zero). The resulting voltage between the two inner electrodes was recorded during 1 ms before and 12 or 30 μs after cutting off the current. A sampling rate of 10 MHz was used. IS measurements were obtained by applying, between the two outer electrodes, a sinusoidal current of amplitude 50 μA with a frequency ranging from 1 MHz to 1 kHz (16 discrete frequencies logarithmically spaced). The AutoLab PGSTAT302N or PGSTAT204 Potentiostat/Galvanostat (Eco-Chemie) with the FRA32M module were used interchangeably to obtain the bioimpedance measurements. Each instrument was controlled by a computer and driven by NOVA software.

In each of the 3 rats, 5 recordings were acquired in the cervical spinal cord using the CIM with another final recording using the classical IS technique to corroborate the experimental data. Then, the same protocol was repeated in the left TS muscle. Only the EEC parameters obtained through the CIM were used for the statistical analysis.

Data analysis. Statistical analysis was performed with the statistical package for Sciences Sigma Plot 11.0 (Inc, Chicago, IL). The EEC parameters were expressed as the mean value of the five trials ± the standard error of the mean (SEM). Comparisons between TS muscle and spinal cord were carried out using Student's t-test or the Mann Whitney Rank Sum's Test. The statistical significance levels were defined as follows: $p<0.05$*, $p<0.01$**, and $p<0.005$***.

Results and Discussion

Figures 3a and 3b show typical transient-voltage responses from the rat spinal cord and striated muscle tissues, respectively. The shape of the resulting voltage is similar to that predicted theoretically in Figure 1c. For the sake of clarity, only the samples taken every 0.2 or 0.4 μs are shown in Figures 3a and 3b, respectively. The previous steady state is shown during the 1 μs preceding the current interruption. Figures 3a and 3b also show the cell-membranes discharge during the interval $t=0^+$ to 12 or 30 μs, respectively. The parameter values listed in Table I were obtained by applying the procedure outlined previously. There is excellent agreement between the experimental and simulated data. For comparison purposes, we have also obtained the parameter values of the EEC of Figure 1a from IS measurements (NOVA software). Typical Nyquist plots (including experimental and simulated impedance data) are shown in Figures 3c (spinal cord) and 3d (TS muscle). Simulated im-

pedance spectra have been obtained using the EEC of Figure 1a and the parameter values given in Table I. The parameter values of the EEC obtained using the CIM are remarkably close to those found with the IS technique. Note that the measurement acquisition time (~1 ms) using the CIM is much shorter than that of the conventional bioimpedance measurements (~30 s). The value of the current (50 μA) was sufficiently small to ensure linear operation of the biological tissue and sufficiently large to allow an acceptable signal-to-noise relation without causing damage to the tissue.[6]

We have used a four-electrode arrangement in a straight line with an identical separation distance of 4 mm. The current injected between the two outer electrodes generates a potential distribution, which is frequency-dependent, in the tissue. The parameter values of the EEC of Figure 1a depend not only on the electrical properties of the tissue but also on the geometry of the measuring system.[12] The question of how the parameter values of the EEC change with the interelectrode distance or the insertion depth is solved very effectively by using field theory,[20] which is not the case here.

Figure 4a shows that the average R_I of the spinal cord almost doubled the average R_I of the TS muscle (131.037±2.108 Ω versus 55.706±1.465 Ω respectively; Mann-Whitney Rank Sum Test, p=0.016). The relationship between the average R_E of the spinal cord and that of the TS muscle is quite similar (Figure 4b), whereas the gap between them, though statistically significant, is smaller (253.889±2.049 Ω versus 192.067±0.737 Ω respectively; t-Test, p=0.011). The morphological heterogeneity of the spinal cord tissue compared to the striated muscle with axons of different sizes and with multiple areas of myelin sheaths interspersed with the nodes of Ranviere, which represent the alternation of insulator zones with others of good conductivity and different passive electrical properties,[21] could partially explain this phenomenon. It is worth mentioning that in our experimental set-up, the edge of some of the recording electrodes placed in the spinal cord could be touching the bone of the vertebral body underneath. Moreover, the duramater over the spinal cord must be removed prior to electrode insertion, releasing the CSF and creating a highly conductive environment within the spinal cord,[19,20] which is not to present within the striated muscle during the recordings.

R_E was significantly higher than the R_I for both spinal cord (mean R_I 131.037±2.108 Ω; mean R_E 253.889±2.050 Ω; t-Test, p<0.001) and TS muscle (mean R_I 55.706±1.465 Ω; mean R_E 192.067±0.737 Ω; Mann-Whitney Rank Sum Test, p=0.029) tissues. In a previous study with rat *ex vivo* TS muscle tissue,[6] we found a noticeably higher R_E (231.3 Ω). Although in both studies the target tissue was the same and the recordings were made with a similar set-up, the tissue temperature was not measured. Both *ex vivo* and *in vivo* recordings were made in a surgical area at room temperature (24 ºC), but the *ex vivo* TS muscle had been previously kept at 4 ºC after perfusion with paraformaldehyde 4% solution, whereas the *in vivo* TS muscle was maintained at 36 ºC with the aid of a thermal pad during data acquisition. In our opinion, the main difference between these two experimental designs is the muscle vascularization state. Whereas in *ex vivo* TS the perfusion process had fixed the blood vessels, in the anesthetized rats the TS vascularization was profuse and its blood vessels retained the ability to modify the muscle blood supply, so the higher the blood supply the lower the R_E.[22]

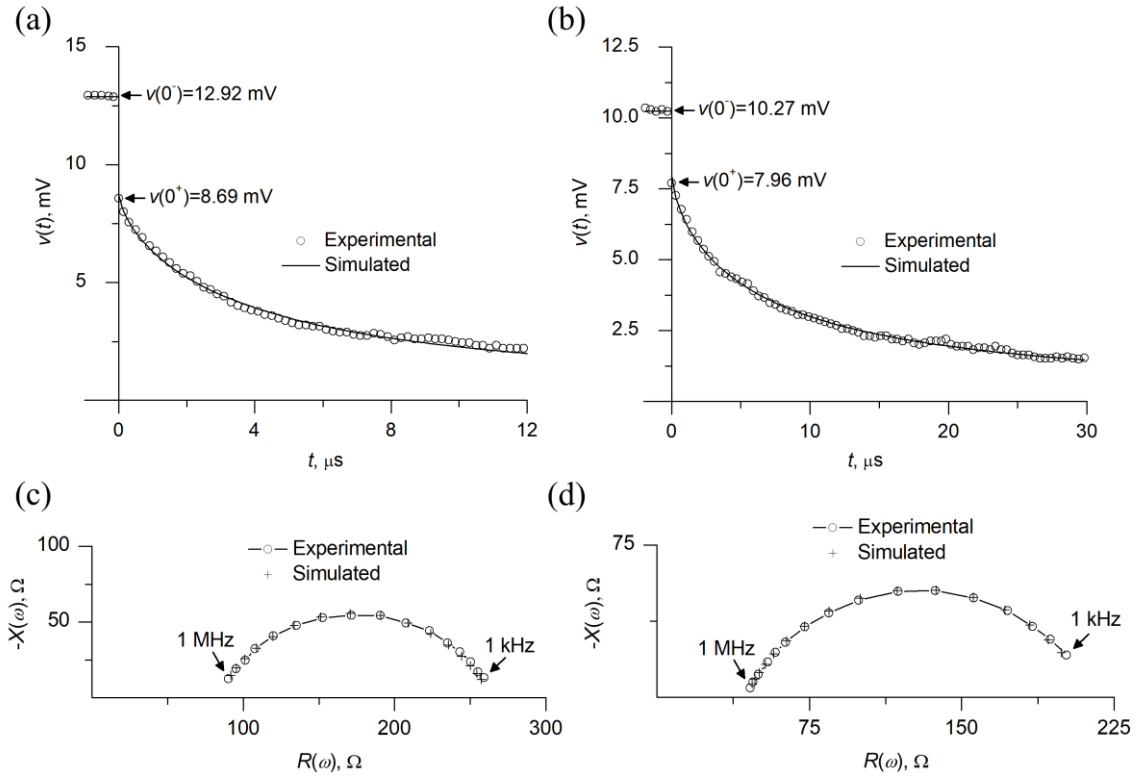

Figure 3. Experimental and simulated results. Representative waveforms of the transient-voltage response for (a) the spinal cord and (b) the triceps surae (TS) muscle, using the current interruption method (CIM). Nyquist plots for (c) the spinal cord and (d) the striated muscle. R(ω) and X(ω) are resistance and reactance, respectively; ω is the angular frequency (ω=2πf where f is the frequency).

Table I. Parameter values of the EEC shown in Figure 1a, obtained using the current interruption method (CIM) and bioimpedance measurements. Distributed time constants (τ) are also included.

Biological tissue	Measurement method	R_I (Ω)	R_E (Ω)	Q_M (nF $s^{\alpha-1}$)	α	τ (μs)
Spinal cord	CIM	125.78	258.39	420.67	0.71	4.57
	Bioimpedance measurements	119.89	264.32	451.81	0.70	4.25
Striated Muscle	CIM	59.61	205.40	1156.94	0.72	13.19
	Bioimpedance measurements	54.26	213.81	1259.87	0.71	12.90

The average α spinal cord value was significantly lower than that of the TS muscle ($0.651\pm9.244\times10^{-3}$ versus $0.665\pm9.349\times10^{-4}$ respectively; t-Test, p=0.001) (see Figure 4c). As the α value quantifies the capacitive behavior of a particular tissue fragment considered globally (α=1, pure capacitor), this difference could also be due to the non-homogeneous distribution of the myelin sheaths along the axons, as opposed to the more homogeneous distribution of the lipid bilayer within the muscular cell membrane. This interpretation, although attractive, is speculative and should be carefully verified with other experimental set-ups of subcellular size and resolution.

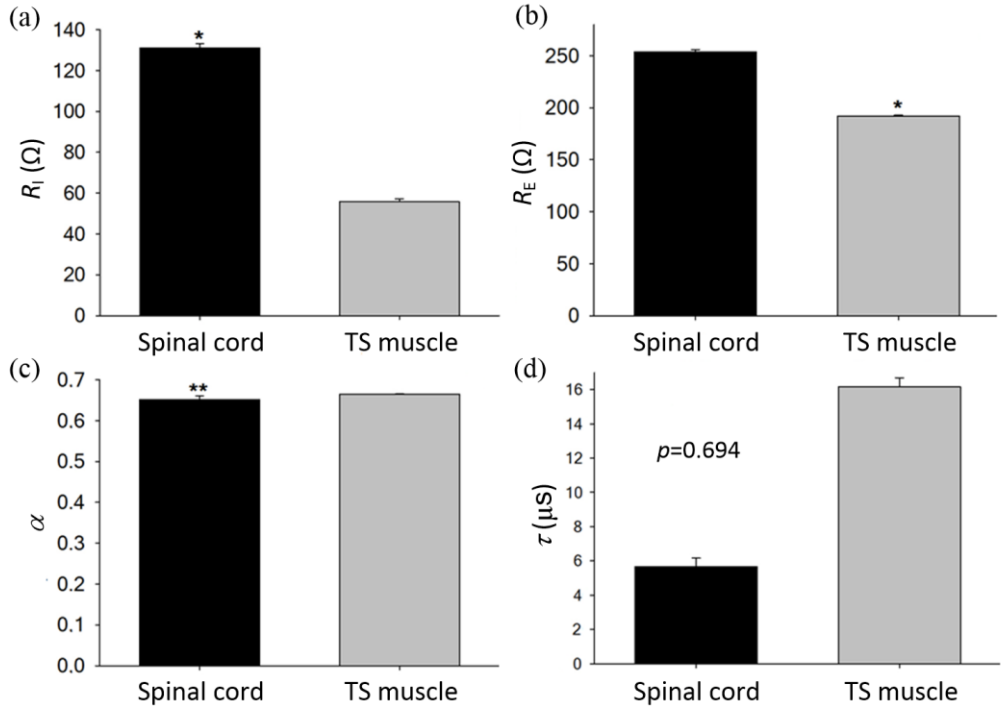

Figure 4. Electrical equivalent circuit (EEC) parameter values of rat spinal cord and triceps surae (TS) muscle obtained using the current interruption method (CIM). (a) R_I; (b) R_E; (c) α; and (d) τ average values. *p<0.05. **p<0.001.

Figure 4d represents the average spinal cord and TS τ ± SEM values (Mann-Whitney Rank Sum Test, p=0.694). Although we have not found statistically significant differences between the average τ values of the spinal cord and the TS muscle (Figure 4d), this apparent similarity (p=0.694), which would indicate a similar electrical activation speed for both tissues, might not be accurate, since the calculation of the τ value takes into account the α value and therefore, its error could be transmitted to the global value of τ. Thus, this "apparent similarity" should be treated with great caution.

Conclusions

The CIM is able to detect real-time differences in the EEC parameter values, modeling *in vivo* electrical properties of the spinal cord and TS muscle of the normal rat. The combination of high speed data acquisition that CIM permits, and the knowledge on the specific and differential electrical properties of these two target tissues will help to optimize the design of chronically implantable neuroprostheses and the electrical stimulation protocols.

Acknowledgements

This study was funded by the Ministerio de Economía, Industria y Competitividad (Project MTM2016-80539-C2-1-R). E. Hernández-Balaguera expresses his gratitude to the Universidad de Castilla-La Mancha (01110/541A) for the Pre-PhD contract granted to him.

References

1. J. L. Collinger, S. Foldes, T. M. Bruns, B. Wodlinger, R. Gaunt, and D. J. Weber, *J. Spinal Cord Med.*, **36**, 258 (2013).
2. D. R. Merrill, M. Bikson, and J. G. R. Jefferys, *J. Neurosci. Methods*, **141**, 171 (2005).
3. S. M. Wellman, J. R. Eles, K. A. Ludwig, J. P. Seymour, N. J. Michelson, W. E. McFadden, A. L. Vazquez, and T. D. Y. Kozai, *Adv. Funct. Mater.*, **28**, 1701269 (2018).
4. J. W. Salatino, K. A. Ludwig, T. D. Y. Kozai, and E. K. Purcell, *Nature Biomed. Eng.*, **1**, 862 (2017).
5. E. López-Dolado, A. González-Mayorga M. C. Gutiérrez, and M. C. Serrano, *Biomaterials*, **99**, 72 (2016).
6. E. Hernández-Balaguera, E. López-Dolado, and J. L. Polo, *RSC Adv.*, **6,** 22312 (2016).
7. S. Lempka and C. McIntyre, in *Encyclopedia of Computational Neuroscience*, D. Jaeger and R. Jung, Editors, p. 374, Springer, New York (2014).
8. C. Bédard, J.-M. Gomes, T. Bal, and A. Destexhe, *J. Integr. Neurosci.*, **16**, 3 (2017).
9. T. Wagner, U. Eden, J. Rushmore, C. J. Russo, L. Dipietro, F. Fregni, S. Simon, S. Rotman, N. B. Pitskel, C. Ramos-Estebanez, A. Pascual-Leone, A. J. Grodzinsky, M. Zahn, and A. Valero-Cabré, *Neuroimage*, **85**, 1048 (2014).
10. S. F. Lempka, B. Howell, K. Gunalan, A. G. Machado, and C. C. McIntyre, *Clin. Neurophysiol.*, **129**, 731 (2018).
11. F. Preda, C. Cavandoli, C. Lettieri, M. Pilleri, A. Antonini, R. Eleopra, M. Mondani, A. Martinuzzi, S. Sarubbo, G. Ghisellini, A. Trezza, M. A. Cavallo, A. Landi, and M. Sensi, *Eur. J. Neurol.*, **23**, 190 (2016).
12. S. Grimnes and O. G. Martinsen, *Bioimpedance and Bioelectricity Basics*, Academic Press, London (2015).
13. C. Gabriel, S. Gabriel, and E. Corthout, *Phys. Med. Biol.*, **41**, 2231 (1996).
14. S. Gabriel, R. W. Lau, and C. Gabriel, *Phys. Med. Biol.*, **41,** 2251 (1996).
15. M. T. Wilson, M. Elbohouty, L. J. Voss, and D. A. Steyn-Ross, *Physiol. Meas.*, **35,** 267 (2014).
16. N. K. Logothetis, C. Kayser, and A. Oeltermann, *Neuron*, **55,** 809 (2007).
17. S. F. Lempka, S. Miocinovic, M. D. Johnson, J. L. Vitek, and C. C McIntyre, *J. Neural Eng.*, **6**, 046001 (2009).
18. J. C. Williams, J. A. Hippensteel, J. Dilgen, W. Shain, and D. R. Kipke, *J. Neural Eng.*, **4,** 410 (2007).
19. M. Utz, J. W. Miller, C. G. Reddy, S. Wilson, K. O. Abode-Iyamah, D. C. Fredericks, G. T. Gillies, and M. A. Howard III, *bioRxiv*, DOI: 10.1101/252965.
20. G. R. Hernández-Labrado, J. L. Polo, E. López-Dolado, and J. E. Collazos-Castro, *Med. Biol. Eng. Comput.*, **49**, 417 (2011).
21. A. G. Richardson, C. C. Mclntyre, and W. M. Grill, *Med. Biol. Eng. Comput.*, **38**, 438 (2000).
22. Y. Wan, A. Borsic, J. Heaney, J. Seigne, A. Schned, M. Baker, S. Wason, A. Hartov, and R. Halter, *Med. Phys.*, **40**, 063102 (2013).

4.2.3 Artículo nº 3

Autores: E. Hernández-Balaguera, J. L. Polo
Título: A generalized procedure for the coulostatic method using a constant phase element
Revista: Electrochimica Acta
Volumen: 233
Páginas: 167-172
Año: 2017
Web: https://www.sciencedirect.com/science/article/pii/S0013468617304899

Abstract

The coulostatic method has been successfully used in the study of electrode processes. In the literature, the technique is explained on the premise that the step-charge is transferred to an ideal interfacial capacitance. Here, for the first time, we have generalized the coulostatic test method by considering a non-ideal interfacial capacitance modeled by a constant phase element (CPE), which agrees with the relaxation processes observed experimentally. The methodology proposed allows one to determine the parameters of a modified Randles circuit consisting of a resistor in series with the parallel combination of a CPE and another resistor. A set of useful expressions for the transient response to a rectangular current pulse is derived using fractional calculus and circuit theory. In addition, we analyze the width of the pulse required to guarantee an efficient coulostatic approach, that is, the total charge associated with the current pulse is transferred to the CPE. Both the method proposed and the impedance spectroscopy (IS) technique (for comparative purposes) are used to study a two-electrode setup consisting of two platinum (Pt) electrodes in contact with a phosphate-buffered saline (PBS) solution.

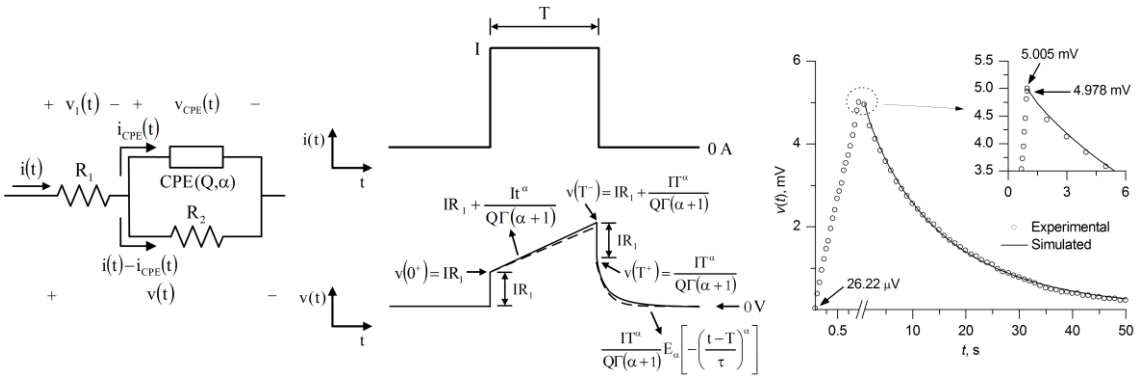

Keywords: Coulostatic method, fractional calculus, constant phase element, biomedical interfaces, impedance spectroscopy.

1. Introduction

The coulostatic technique [1-3] has been widely employed to study and characterize electrode reactions [4-8]. The method assumes exponential decay in response to the coulostatic pulse. This approach is reasonable for electrode systems whose behavior is close to that of a Randles circuit, which assumes an ideal interfacial capacitance. Note that the diffusion element is omitted here. However, transient decays observed experimentally deviate from this ideal exponential behavior and new functions need to be introduced for an accurate description of the electrode interface. In this paper, the ideal capacitor for modelling the interfacial capacitance has been replaced by a constant phase element (CPE). This latter circuit element takes into account the space distribution of the electrical properties of an electrode interface [9], which agrees with the relaxation processes observed experimentally. In turn, the introduction of a CPE involves the mathematical tools of fractional calculus and the handling of distributed electrical circuits [9-13].

Specifically, consider the lumped-parameter electrical circuit of Fig. 1(A), comprising a resistance (R_1) in series with the parallel combination of an ideal capacitor (C) and a resistance (R_2). v(t) and i(t) are the voltage and current, respectively, at the terminals of the circuit. Note that these terminals correspond to the available external connections of the system under study. We have also labelled the currents through the capacitor C and the resistor R_2 as $i_C(t)$ and $i(t)-i_C(t)$, respectively. $v_C(t)$ is the voltage across C or R_2. The voltage of the resistor R_1 is denoted by $v_1(t)$. Note that the elements of the electrical equivalent circuit (EEC) involve a general notation which can be adapted to the specific interface or process being modelled.

Now, assume that an adequate current pulse i(t) injects an amount of electrical charge into the capacitor C. Immediately after this, C will discharge through R_2. Importantly, this exponential-decay voltage v(t) depends only on the electrical properties modelled by the subcircuit C-R_2. Indeed, the open-circuit voltage v(t) at the terminals of the EEC of Fig. 1(A) only involves the voltage $v_C(t)$. Since the current through R_1 is zero, there will be no voltage drop across it, which is an advantage of the coulostatic method when the solution is poorly conducting. Note that to know the value of R_1, the voltage v(t) should be obtained just before and just after the step change at the leading or trailing edge of the pulse (see below).

The question then is: how is a step-charge injected into the capacitor (C)?. Theoretically speaking, a finite amount of electric charge is transferred to C instantaneously if the input excitation is the unit impulse or delta function δ(t) which has "infinite" height and "zero" duration [2,3,14]. This singular function must be understood from the notion of distribution or generalized function [14]. It should be noted, however, that the delta function is not physically realizable and a practical implementation of an impulse excitation is that of a sufficiently short pulse compared to the time constants of the circuit (see below). In this paper, we make use of rectangular current pulses whose durations are sufficiently small.

The EEC of Fig. 1(B) is similar to that of Fig. 1(A) except that the ideal capacitor has been replaced by a CPE. $v_{CPE}(t)$ and $i_{CPE}(t)$, the voltage and current, respectively, of the CPE, are related by

$$i_{CPE}(t)=Q\frac{d^{\alpha}v_{CPE}(t)}{dt^{\alpha}} \qquad (1)$$

where Q has the units of (farads)×(seconds)$^{\alpha-1}$ with $i_{CPE}(t)$ in amperes, $v_{CPE}(t)$ in volts, and t in seconds. d^{α}/dt^{α} ($0<\alpha<1$) is the fractional-order derivative of order α [11]. In the case $\alpha=1$, Eq. (1) yields the current-voltage relation for an ideal capacitor ($Q=C$), $i_C(t)=C(dv_C(t)/dt)$ -see Fig. 1(A)-.

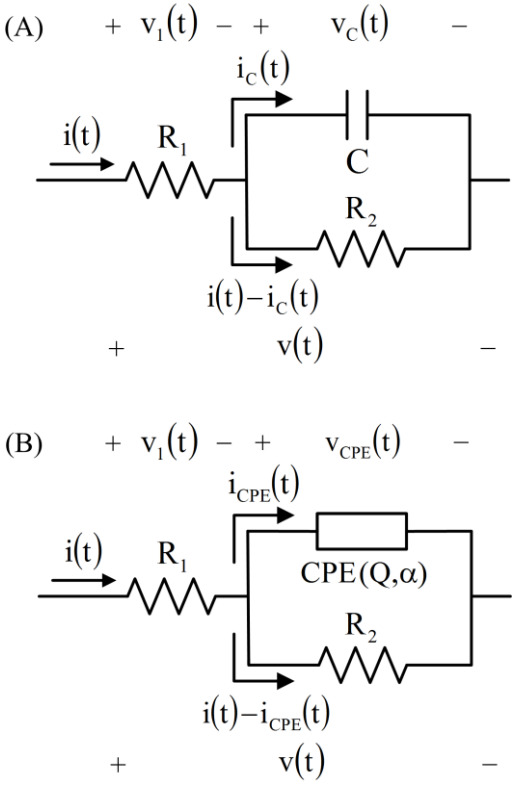

Figure 1. Electrical equivalent circuit (EEC) involving two resistors and (A) an ideal capacitor or (B) a CPE.

In the literature, there exists a range of published time-based methods (transient responses to galvanostatic pulses or voltage steps) for the determination of EEC parameters describing non-ideal interfacial behavior [15-20]. An advantage of these methods over the conventional impedance technique is a reduction in the measurement time, which may become one of the most critical requirements. Indeed, the measurement acquisition time should be sufficiently short to ensure that the time-invariant assumption for the electrode process is satisfied. Specifically, non-exponential relaxations are described by the Kohlrausch-Williams-Watt (KWW) function (stretched exponential) or a generalized Cauchy-Lorentz function [15,16,18-20]. Moreover, this latter function was found by considering the discharge of an ideal capacitor through a Tafel element acting as a non-linear resistor [20].

We have used the Mittag-Leffler function (natural response of the EEC of Fig. 1(B)) to describe the non-ideal exponential decay in response to a coulostatic pulse. Interestingly, the method proposed has the inherent advantage of being a coulostatic test [3]. Note that the electrode is perturbed for only a very short time (pulse of duration much shorter than the electrical inertia exhibited by the electrode) and the natural response depends only on the electrical properties of the electrode itself. The pulse only serves the purpose of injecting a controlled step-charge.

The aim of this paper was to generalize the coulostatic test method to determine the parameters of the modified Randles circuit shown in Fig. 1(B), which involves a CPE. We

derive the mathematical expressions for the transient-voltage response to a rectangular current pulse and, furthermore, analyze the width of the pulse required to perform an efficient coulostatic approach. The procedure proposed has been used to study a platinum/phosphate-buffered saline solution/platinum (Pt/PBS/Pt) system, which constitutes a two-electrode setup of biomedical interest. Indeed, the PBS solution can be viewed as a simple tissue model and the Pt/PBS system is a typical electrode-electrolyte interface in biomedical applications [18,21]. We have also checked the consistency of these results by using the impedance spectroscopy (IS) technique.

2. Theory

As mentioned earlier, we study the behaviour of the circuit of Fig. 1(B) in response to the current pulse shown in Fig. 2(A). Then, from the expression of the charge transferred to the CPE, the condition for an efficient coulostatic approach is obtained. Note that the theory of linear time-invariant (LTI) circuits [14] is used throughout the paper. Before going further, we introduce the one (α) and two-parameter (α,β) expressions of the Mittag-Leffler function, which permit mathematical descriptions of fractional (non-exponential) relaxation processes [10].

$$E_{\alpha}\left[-\left(\frac{t}{\tau}\right)^{\alpha}\right]=\sum_{k=0}^{\infty}\frac{\left[-\left(\frac{t}{\tau}\right)^{\alpha}\right]^{k}}{\Gamma(\alpha k+1)} \quad \alpha>0 \tag{2}$$

$$E_{\alpha,\beta}\left[-\left(\frac{t}{\tau}\right)^{\alpha}\right]=\sum_{k=0}^{\infty}\frac{\left[-\left(\frac{t}{\tau}\right)^{\alpha}\right]^{k}}{\Gamma(\alpha k+\beta)} \quad \alpha>0,\ \beta>0 \tag{3}$$

where τ is the time constant and Γ is the gamma function. Note that if $\alpha=1$, Eq. (2) is the MacLaurin series for the exponential function, i.e., $E_1(-t/\tau)=e^{-t/\tau}$.

2.1. Current pulse response

Before proceeding, it should be pointed out that the voltages and currents found are specified for the polarity references shown in the EECs of Fig. 1. This conforms to the standard notion used in circuit theory. Without loss of generality, let us consider the EEC of Fig. 1(B) with an initially uncharged CPE. Next, we shall find the expression for the voltage response v(t) when the input current i(t) is the rectangular pulse of width T and height I, shown in Fig. 2(A). Just after the step change at the leading edge of the pulse (at time $t=0^+$), the voltage $v(0^+)$ is

$$v(0^+)=IR_1 \tag{4}$$

Indeed, it is assumed that the CPE voltage cannot change abruptly, so that the voltage across it, 0 V, just before ($t=0^-$) and just after ($t=0^+$) the step change are equal, that is, $v_{CPE}(0^-)=v_{CPE}(0^+)=0$ V. Thus, $v(0^+)=v_1(0^+)+v_{CPE}(0^+)=v_1(0^+)=I\times R_1$. Note the jump discontinuity at t=0, $v(0^+)-v(0^-)=I\times R_1$, which is shown in Fig. 2(B). Since the uncharged CPE acts as a short circuit ($v_{CPE}(0^+)=0$ V), there can be no current in R_2, and all the current I flows

through the CPE (i.e., $i_{CPE}(0^+)=I$). Now, the CPE begins to charge and its current $i_{CPE}(t)$ decays from I toward zero (CPE fully charged acts as an open circuit) and, correspondingly, v(t) rises from $I\times R_1$ toward $I\times(R_1+R_2)$. Circuit theory [14] and fractional calculus [10-13] shows that these decay and rise processes are described by the one-parameter Mittag-Leffler function (see Eq. (2)), according to the following relationships:

$$i_{CPE}(t)=IE_\alpha\left[-\left(\frac{t}{\tau}\right)^\alpha\right] \quad 0<t<T \tag{5}$$

$$v(t)=IR_1+IR_2\left(1-E_\alpha\left[-\left(\frac{t}{\tau}\right)^\alpha\right]\right) \quad 0<t<T \tag{6}$$

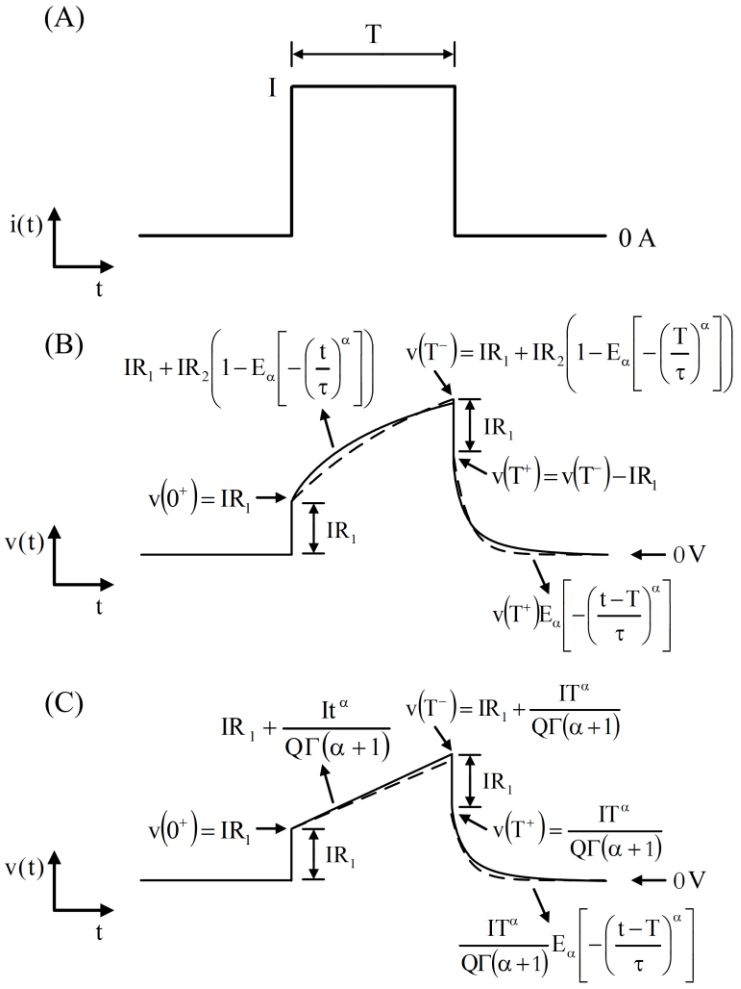

Figure 2. Responses to the rectangular current pulse. (A) Rectangular current pulse of width T and height I. (B) Pulse responses of the EECs shown in Fig. 1(A) -dashed line- and Fig. 1(B) -solid line-. (C) Coulostatic approach.

To find the time constant (τ), the current source which supplies the current pulse is replaced by an open circuit and the CPE only "sees" the resistance R_2. Thus, τ is the product $R_2\times Q$ raised to the power $1/\alpha$ [11].

$$\tau=(R_2Q)^{1/\alpha} \tag{7}$$

Fig. 2(B) shows the waveform of the resulting voltage v(t) for $0<t<T$. The specific case in which $\alpha=1$ (ideal capacitor) has also been plotted (see dashed line). The process of charging the CPE is stopped at time $t=T$ when the negative step change of the pulse occurs (from T^- to T^+) and the voltage v(t) has a jump discontinuity. The value of $v(T^-)$ is obtained from Eq. (6) where $t=T$:

$$v(T^-)=IR_1+IR_2\left(1-E_\alpha\left[-\left(\frac{T}{\tau}\right)^\alpha\right]\right) \tag{8}$$

Since $v(t)=v_1(t)+v_{CPE}(t)$ -see Fig. 1(B)- and $v_{CPE}(t)$ is a continuous function (see below), the magnitude of the jump $v(T^+)-v(T^-)$ is due to $v_1(T^+)-v_1(T^-)=-I\times R_1$, resulting in

$$v(T^+)=v(T^-)-IR_1 \tag{9}$$

Substituting for $v(T^-)$ from Eq. (8) enable us to express $v(T^+)$ as

$$v(T^+)=IR_2\left(1-E_\alpha\left[-\left(\frac{T}{\tau}\right)^\alpha\right]\right) \tag{10}$$

At time $t=T^+$, the CPE begins to discharge through R_2 and the voltage v(t) is given by

$$v(t)=v(T^+)E_\alpha\left[-\left(\frac{t-T}{\tau}\right)^\alpha\right] \quad t>T \tag{11}$$

Note that the decay of v(t) involves the same time constant (see Eq. (6)) as the charge process. Note also that for $t>T$ the voltage drop across R_1 is zero and, thus, the measured voltage v(t) is indeed the CPE voltage. The waveform of the resulting voltage v(t) for $t>T$ is also sketched in Fig. 2(B). The dashed line indicates v(t) for $\alpha=1$ (exponential behaviour). The fractional relaxation exhibits a faster (slower) decay than the exponential, for short (long) times (refer to Fig. 2(B)) [11].

2.2. The coulostatic approach

Now we must ensure that the width (T) of the current pulse is sufficiently short so that its total charge ($I\times T$) is transferred to the CPE. Just after applying the pulse (at time $t=T^+$), the stored charge in the CPE, denoted by $q_{CPE}(T)$, can be found by integrating Eq. (5) from $t=0$ to $t=T$ (remember that the CPE is initially discharged),

$$q_{CPE}(T)=ITE_{\alpha,2}\left[-\left(\frac{T}{\tau}\right)^\alpha\right] \tag{12}$$

Using Eq. (3), the Mittag-Leffler function of Eq. (12) can be expanded in a power series as follows:

$$q_{CPE}(T)=IT\left[1-\frac{\left(\frac{T}{\tau}\right)^\alpha}{\Gamma(\alpha+2)}+\frac{\left(\frac{T}{\tau}\right)^{2\alpha}}{\Gamma(2\alpha+2)}-\frac{\left(\frac{T}{\tau}\right)^{3\alpha}}{\Gamma(3\alpha+2)}+\ldots\right] \tag{13}$$

We conclude that if $(T/\tau)^{\alpha}/\Gamma(\alpha+2)<<1$ (which is rearranged to yield Eq. (14)), the stored charge in the CPE just after applying the pulse is $q_{CPE}(T)\sim I\times T$, whose value is equal to the charge injected by the current pulse.

$$T\ll\tau[\Gamma(\alpha+2)]^{1/\alpha} \tag{14}$$

Specifically, let us consider that T is about an order of magnitude smaller than the quantity on the right-hand side of Eq. (14). An upper limit (T_{max}) on the values of T for an efficient coulostatic approach is then given by

$$T_{max}=\tau[0.1\Gamma(\alpha+2)]^{1/\alpha} \tag{15}$$

Note that if $\alpha=1$ (CPE is an ideal capacitor), Eq. (15) provides $T_{max}=\tau/5$ which is an interesting result. In effect, for $T\leq\tau/5$ the current pulse is a practical implementation of the impulse function and the total charge injected is assumed to be transferred to the capacitor of the EEC of Fig 1(A).

Assume that the condition of Eq. (14) is satisfied. We expand Eq. (6) in a series (see Eq. (2)) and consider the first two non-vanishing terms,

$$v(t)=IR_1+\frac{It^{\alpha}}{Q\Gamma(\alpha+1)} \tag{16}$$

$v(T^{-})$ is now expressed as

$$v(T^{-})=IR_1+\frac{IT^{\alpha}}{Q\Gamma(\alpha+1)} \tag{17}$$

Substituting this value into Eq. (9) gives

$$v(T^{+})=\frac{IT^{\alpha}}{Q\Gamma(\alpha+1)} \tag{18}$$

From a circuit-theory point of view, there is no theoretical lower limit (T_{min}, $T_{min} > 0$) on the values of T. However, there is a limit imposed by the minimum width of the pulse that can be generated by the experimental setup.

Finally, Eq. (11) is rewritten as

$$v(t)=\frac{IT^{\alpha}}{Q\Gamma(\alpha+1)}\ E_{\alpha}\left[-\left(\frac{t-T}{\tau}\right)^{\alpha}\right] \quad t>T \tag{19}$$

Fig. 2(C) shows the output waveform v(t) for the coulostatic approach, including the specific case in which $\alpha=1$. Note that the portion of v(t) for $0<t<T$ (pulse duration) seems almost proportional to the input, that is, the CPE is ideally "frozen" in time during the application of the pulse which is the basis of the coulostatic method.

Recall that Eqs. (4)-(19) have been obtained using the theory of LTI circuits and, thus, the magnitude I of the input current should ensure the linear operation of the electrode

system studied. If the linear region is bounded by the lower and upper limits (I_- and I_+, respectively) on the value of I, the following constraint should be satisfied:

$$I_- \leq I \leq I_+ \tag{20}$$

Note that a very low value of I could result in a magnitude of the jump $v(T^+)$-$v(T^-)$ smaller than the resolution of the measuring device.

To summarize, in order to obtain the values of the parameters of the EEC of Fig. 1(B) from an experimental waveform v(t), the following procedure is performed: (i) α and τ are determined by fitting the transient-voltage response v(t) for t>T to Eq. (19); (ii) Q is obtained from the value of $v(T^+)$ and using Eq. (18); (iii) R_2 is now calculated from Eq. (7); (iv) R_1 can be found from Eq. (4) or from Eq. (9).

3. Experimental

The experimental setup consisted of two identical platinum electrodes (surface area of 0.5 cm^2) in parallel-opposed configuration and separated by a ~ 1.5 cm gap. The rectangular chamber was filled with an aqueous 5 mM potassium phosphate-buffered saline (PBS, Milli-Q water purified to 18.2 $M\Omega/cm^2$ with 9 g NaCl, 0.8 g $Na_2HPO_42H_2O$ and 0.14 g KH_2PO_4 added per liter). All the experiments were carried out at a room temperature.

An AutoLab PGSTAT302N Potentiostat/Galvanostat (Eco-Chemie), combined with the ADC10M module, was used to implement the coulostatic method. Under galvanostatic control, rectangular pulses of different heights, of 200, 400, 600, 800, and 1000 nA, and durations of 0.1 and 1 s were injected into the two-electrode setup. The voltage responses were recorded during 50 s, beginning at the instant the pulse is applied until the time at which the subsequent relaxation process approaches to zero. A sampling rate of 20 kHz was used, and all the experiments were repeated twice.

Impedance measurements were carried out using the AutoLab PGSTAT302N Potentiostat/Galvanostat (Eco-Chemie). Sinusoidal signals of 5, 25, and 50-mV amplitudes were applied at 31 logarithmically spaced frequencies (5 steps per decade) from 10 kHz to 10 mHz. The tests were repeated twice. The instrument was controlled by a computer and driven by NOVA software.

4. Results and discussion

The experimental-voltage waveform between the two identical electrodes of the Pt/PBS/Pt system was obtained, in response to the current pulse of 200-nA height (I=200 nA) and 1-s width (T=1 s). Fig. 3(A) shows the output-voltage waveform scaled by a factor of 0.5 to consider the sum of the voltages across a unique Pt/PBS interface and the half-volume of electrolyte. Note that we consider the small-signal operation of the symmetrical two-electrode setup at the zero-dc operating point.

The graphical representation of v(t) has been expanded and labeled to reveal details. The shape of the waveform is similar to that predicted theoretically (see Fig. 2(C)) showing: (i)

the value of $v(0^+)$, indicated by an arrowhead; (ii) the portion during which the charge is transferred to the CPE, shown on an expanded scale, $0<t<1$ s; (iii) the jump discontinuity. The values of $v(T^-)$ and $v(T^+)$ have been indicated by arrowheads on an expanded view (see the inset to Fig. 3); and (iv) the voltage relaxation for $t>T$. Since the magnitude of $I\times R_1$ is very small (~26 μV) and is extremely difficult to visualize in Fig. 3(A), the theoretically predicted waveform of Fig. 2(C) is redrawn in Fig. 3(B) and relabeled to correspond to the experimental values obtained. Table 1 lists the values of the parameters of the EEC shown in Fig. 1(B). They have been obtained by applying the procedure outlined in Section 2.2.

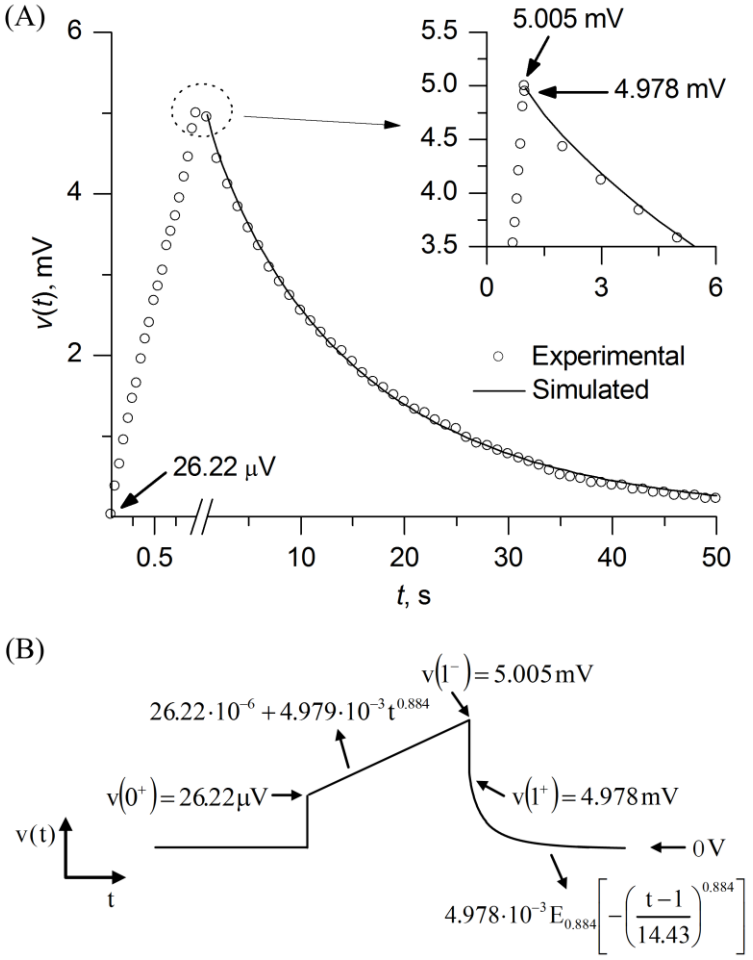

Figure 3. Experimental and simulated results. (A) Waveforms of the resulting voltage in response to the charge injection (coulostatic method) for the Pt/PBS interface. (B) Fig. 2(C) relabeled in correspondence with the experimental values obtained.

Note that the parameter values have been normalized to the electrode area by considering the current density (pulse of 400-nA/cm^2 height and 1-s width). The value of τ is also included in Table 1. The values found (see Table 1) are similar to those previously reported in the literature [21]. The fitting procedure was performed using a routine in MATLAB [22]. The experimental and simulated data are in excellent agreement. An average error of 1.5% was obtained by using the function: $\frac{100}{N\, v_{exp}^{max}}\sum_i |v_{exp}(t_i)-v_{sim}(t_i)|$, where $v_{exp}(t_i)$ and $v_{sim}(t_i)$ are the experimental and simulated voltages at time t_i, respectively, v_{exp}^{max} is the maximum value of $v_{exp}(t_i)$, and N is the total number of points. Note that the condition of Eq. (14) is satisfied and thus a consistent solution is obtained. In effect, since τ~14 s and T=1 s,

Eq. (14) gives 1 s << 14 s. A sampling rate of 20 kHz allowed accurate determinations of $v(0^+)$, $v(T^-)$, and $v(T^{+})$. For the sake of clarity, not all the samples taken are shown in Fig. 3(A). We also check that the Pt/PBS/Pt system "feels" that the current is abruptly changed (positive/negative step change at the leading/trailing edge of the pulse), that is, τ is much greater than the rise and fall times of the pulse, as is the case here.

We have also obtained impedance measurements between the two electrodes of the Pt/PBS/Pt system. Recall that impedance $Z(j\omega)$ is a complex number whose real and imaginary parts are the resistance $R(\omega)$ and the reactance $X(\omega)$, that is, $Z(j\omega)=R(\omega)+jX(\omega)$ where j is the imaginary unit and ω is the angular frequency ($\omega=2\pi f$ where f is frequency) [11]. Real and imaginary parts of the impedance have been divided by 2 (the contribution of a unique Pt/PBS interface) and also normalized to the electrode area. The Nyquist plot (refer to Fig. 4) for the Pt/PBS system shows a depressed semicircle. The high-frequency region is also plotted in the inset to Fig. 4. Experimental impedance data were fitted to the EEC shown in Fig. 1(B). The parameter values obtained are listed in Table 1. The time constant, calculated from Eq. (7), is also included. The impedance plot also shows the simulated data, obtained using the EEC of Fig. 1(B) and the parameter values given in Table 1. There is excellent agreement between the experimental and simulated results (average error of 0.1%). We have used the following expression: $\frac{100}{N\, Z_{exp}^{max}}\sum_i |Z_{exp}(j\omega_i)-Z_{sim}(j\omega_i)|$, where $Z_{exp}(j\omega_i)$ and $Z_{sim}(j\omega_i)$ are the experimental and simulated impedance data, respectively, at frequency ω_i, Z_{exp}^{max} is the maximum impedance magnitude of experimental data, and N is the total number of points.

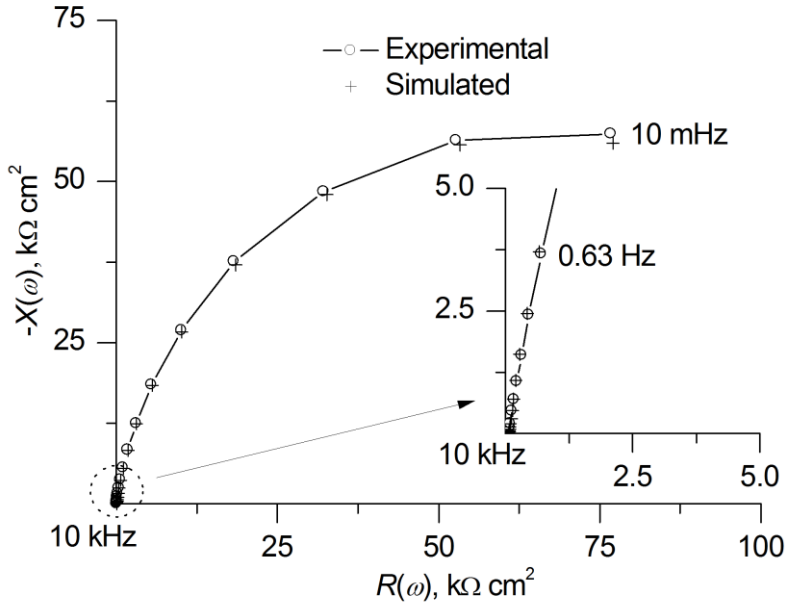

Figure 4. Experimental and simulated results. Nyquist plot for the Pt/PBS interface.

Table 1 also shows that the parameter values obtained using the coulostatic method are remarkably close to those found from IS measurements (discrepancies of less than 10% for the EEC parameters).

It should be mentioned that we have checked the linear operation of the two-electrode setup under a small-signal condition. Rectangular current pulses (duration 1 s) of 200, 400,

600, 800, 1000-nA height were injected into the two-electrode setup. The shape of the transient-voltage responses was identical and the voltage values obtained were directly proportional to the magnitude of the current injected, providing the same parameter values of the EEC. Linearity elsewhere is not checked. Additionally, a pulse duration of 0.1 s was tested and identical EEC parameter values were obtained. For impedance measurements, the linear operation was checked only in the range 5 to 50 mV. Note also that two different inputs (rectangular current pulse and sinusoidal voltage) yielded identical EEC values, guaranteeing linear operation for the electrode interface.

Table 1. Parameter values of the EEC shown in Fig. 1(B), obtained using the coulostatic method and the IS technique. R_1 is the solution resistance, Q and α are the CPE parameters which model the double layer capacitance, and R_2 is the polarization resistance. Values of τ have also been included.

Measurement method	R_1 $\Omega\ cm^2$	Q $\mu F\ cm^{-2}\ s^{\alpha-1}$	α	R_2 $k\Omega\ cm^2$	τ s
Coulostatic method	65.6	84	0.884	126	14.43
Impedance Spectroscopy	63.4	76.8	0.907	131.8	12.83

5. Conclusions

We have generalized the coulostatic test method to determine the parameters of a modified Randles circuit consisting of a resistor in series with the parallel combination of a CPE and other resistor. The procedure proposed has been used to study a Pt/PBS interface. The parameter values of the EEC are remarkably close to those found from the IS technique. The methodology presented may allow a more realistic study of electrode processes from the perspective of fractional calculus and circuit theory.

Acknowledgements

This study was funded the by Junta de Comunidades de Castilla-La Mancha (Project PEII-2014-021-A) and Ministerio de Economía, Industria y Competitividad (Project MTM2016-80539-C2-1-R). E. Hernández-Balaguera expresses his gratitude to the Universidad de Castilla-La Mancha (01110/541A) for the Pre-PhD contract granted to him.

References

[1] P. Delahay, Coulostatic method for kinetic study of fast electrode processes, 1. Theory, J. Phys. Chem. 66 (1962) 2204-2207.

[2] W. H. Reinmuth, Theory of coulostatic impulse relaxation, Anal. Chem. 34 (1962) 1272-1276.

[3] H. P. van Leeuwen, The coulostatic impulse technique: A critical review of its features and possibilities, Electrochim. Acta 23 (1978) 207-218.

[4] D. J. Kooijman, J. H. Sluyters, The galvanostatic single-pulse and the coulostatic impulse methods for the determination of the rate constants of electrode reactions, Electrochim. Acta 12 (1967) 1579-1592.

[5] K. Kanno, M. Suzuki, Y. Sato, An application of coulostatic method for rapid evaluation of metal corrosion rate in solution, J. Electrochem. Soc. 125 (1978) 1389-1393.
[6] V. Dharuman, E. Nebling, T. Grunwald, J. Albers, L. Blohm, B. Elsholz, R. Wörl, R. Hinstche, DNA hybridization detection on electrical microarrays using coulostatic pulse technique, Biosens. Bioelectron. 22 (2006) 744-751.
[7] G. K. Glass, An assessment of the coulostatic method applied to the corrosion of steel in concrete, Corros. Sci. 37 (1995) 597-605.
[8] J. A. González, A. Cobo, M. N. González, S. Feliu, On-site determination of corrosion rate in reinforced concrete structures by use of galvanostatic pulses, Corros. Sci. 43 (2001) 611-625.
[9] E. Barsoukov, J. R. Macdonald, Impedance Spectroscopy: Theory, Experiment, and Applications, John Wiley & Sons, New Jersey, 2005.
[10] I. Podlubny, Fractional Differential Equations, Academic Press, San Diego, 1999.
[11] E. Hernández-Balaguera, E. López-Dolado, J. L. Polo, Obtaining electrical equivalent circuits of biological tissues using the current interruption method, circuit theory and fractional calculus, RSC Adv. 6 (2016) 22312-22319.
[12] R. L. Magin, Fractional calculus in bioengineering, Part 2, Crit. Rev. Biomed. Eng. 32 (2004) 105-193.
[13] E. Hernández-Balaguera, H. Vara, J. L. Polo, An electrochemical impedance study of anomalous diffusion in PEDOT-coated carbon microfiber electrodes for neural applications, J. Electroanal. Chem. 775 (2016) 251-257.
[14] F. F. Kuo, Network Analysis and Synthesis, John Wiley & Sons, New York, 1966.
[15] N. Birbilis, K. M. Nairn, M. Forsyth, Transient response analysis of steel in concrete, Corros. Sci. 45 (2003) 1895-1902.
[16] N. Birbilis, K. M. Nairn, M. Forsyth, On the electrochemical response and interfacial properties of steel-Ca(OH)2 and the steel-concrete system measured using galvanostatic pulses, Electrochim. Acta 49 (2004) 4331-4339.
[17] V. Feliu, J. A. González, S. Feliu, Corrosion estimates from the transient response to a potential step, Corros. Sci. 49 (2007) 3241-3255.
[18] M. T. Ehrensberger, J. L. Gilbert, A time-based potential step analysis of electrochemical impedance incorporating a constant phase element: A study of commercially pure titanium in phosphate buffered saline, J. Biomed. Mater. Res. Part A 93A (2010) 576-584.
[19] R. T. T. Gettens, J. L. Gilbert, The electrochemical impedance of polarized 316L stainless steel: Structure-property-adsorption correlation, J. Biomed. Mater. Res. Part A 90A (2009) 121-132.
[20] M. Haeri, S. Goldberg, J. L. Gilbert, The voltage-dependent electrochemical impedance spectroscopy of CoCrMo medical alloy using time-domain techniques: Generalized Cauchy-Lorentz, and KWW-Randles functions describing non-ideal interfacial behaviour, Corros. Sci. 53 (2011) 582-588.
[21] A. Norlin, J. Pan, C. Leygraf, Investigation of Pt, Ti, TiN, and nano-porous carbon electrodes for implantable cardioverter-defibrillator applications, Electrochim. Acta 49 (2004) 4011-4020.
[22] I. Podlubny, I. Petrás, T. Skovránek, Fitting of experimental data using Mittag-Leffler function, Proceedings of the 13th International Carpathian Control Conference (2012) 578-581.

Capítulo 5

Conclusiones y futuros desarrollos

5 Conclusiones y futuros desarrollos

En este capítulo se exponen las conclusiones alcanzadas en la presente Tesis Doctoral y se sugieren futuras líneas de trabajo.

5.1 Conclusiones

(i) Se han establecido los aspectos teóricos del método de interrupción de corriente (CIM) para la estimación en tiempo real de los parámetros de circuitos eléctricos equivalentes (EECs) de tejidos biológicos descritos por el modelo de Fricke y Morse. Las propiedades capacitivas no ideales del tejido se han modelado utilizando un elemento de fase constante (CPE).

(ii) Se ha implementado *ex vivo* el CIM para estimar los valores de los parámetros de EECs en hígado y músculo estriado de roedor. El CIM mostró ser una herramienta fidedigna para la obtención en tiempo real de dichos parámetros de EECs en tejidos que presentan diferencias histológicas y de excitabilidad. Los resultados obtenidos mediante el CIM se corroboraron utilizando la técnica convencional de espectroscopía de impedancia eléctrica. Además, un análisis histológico permitió asegurar que el CIM no produjo daño adicional en los tejidos.

(iii) Se ha evaluado la potencialidad del CIM para obtener *in vivo* los EECs que modelan el comportamiento eléctrico pasivo de los tejidos excitables del sistema neuromuscular de rata, específicamente de la médula espinal y del músculo tríceps sural. Un análisis estadístico de los valores de los parámetros de los EECs permitió dilucidar su significado fisiológico. Utilizando medidas de impedancia se corroboraron los valores de los componentes de los EECs obtenidos mediante el CIM. En el contexto de las neuroprótesis, los resultados que se muestran son de interés puesto que los dispositivos capaces de evocar respuestas motoras complejas diseñadas para pacientes con enfermedades neurológicas tendrán que actuar tanto sobre el sistema nervioso central (CNS) como sobre los músculos efectores. La combinación de la adquisición de datos a alta velocidad, a partir de medidas eléctricas basadas en la carga y descarga de las membranas celulares, y el conocimiento de las propiedades eléctricas específicas y diferenciales de estos tejidos podría ayudar a optimizar el diseño de las neuroprótesis implantables crónicamente y los protocolos de estimulación eléctrica.

(iv) Utilizando un CPE, se ha generalizado el método de inyección súbita de carga (método "culostático", CM) y se ha aplicado a la caracterización de un sistema "platino/solución de tampón fosfato salino (PBS)/platino". La solución de PBS constituye un simulador muy simplificado de un tejido biológico. Los resultados obtenidos son de interés porque suponen un paso previo para la aplicación del CM en tejidos biológicos, lo que permitiría una reducción drástica del tiempo de exposición del tejido a la corriente y, por ende, del riesgo de lesión.

5.2 Sugerencias sobre futuros desarrollos

(i) Describir mediante medidas eléctricas el tejido neural diferenciando entre sustancia blanca y sustancia gris, y entre tejido normal y con lesión medular. Los parámetros eléctricos permitirían mostrar la correlación con la extensión de la muerte neuronal y la destrucción axonal, para predecir la severidad de la lesión y evaluar su evolución a partir de las modificaciones de las propiedades eléctricas asociadas a la zona bajo estudio. Aunque no se ha incluido en la presente Tesis Doctoral, se han obtenido unos primeros resultados que muestran cómo una lesión incompleta de la médula espinal cervical modifica los parámetros eléctricos de los músculos estriados, dos de ellos localizados en el epicentro de la lesión y otros dos de ellos alejados e inervados por metámeras lumbares.

(ii) Reducir aún más el tiempo de medida y de exposición del tejido a la corriente implementando el método "culostático" o de inyección súbita de carga. Incluso se podrían ensayar medidas utilizando dos electrodos (en lugar de cuatro) analizando los valores de las constantes de tiempo involucradas en la carga de la interfase electrodo/tejido y del propio tejido.

(iii) Adaptar la técnica de interrupción de corriente (CIM) a modelos eléctricos más complicados que el de Fricke y Morse y que permitan obtener una descripción adecuada de estados tisulares más complejos.